MDPI

Review

Metal Nanocluster-Based Biosensors for DNA Detection

Ran He, Sheng Wang, Feiye Ju, Zhao Huang, Yuan Gao, Jing Zhang, Nongyue He * and Libo Nie *

Hunan Key Laboratory of Biomedical Nanomaterials and Devices, College of Life Sciences and Chemistry, Hunan University of Technology, Zhuzhou 412007, China; m22077700021@stu.hut.edu.cn (R.H.); m23077700008@stu.hut.edu.cn (S.W.); m22077700026@stu.hut.edu.cn (F.J.); huang1020@hut.edu.cn (Z.H.); gaoyuan@hut.edu.cn (Y.G.); zhang_jing@hut.edu.cn (J.Z.)
* Correspondence: nyhe@seu.edu.cn (N.H.); nielibo@hut.edu.cn (L.N.)

Abstract: The early detection of genetic diseases is a critical need in modern medicine, underscoring the importance of developing deoxyribonucleic acid (DNA) biosensors. In recent years, metal nanoclusters (MNCs) have demonstrated significant potential as biosensors for DNA detection due to their ultra-small size, excellent photostability, bright photoluminescence, low toxicity and other outstanding properties. This review firstly discusses the characteristics of MNCs, which are effective in the early diagnosis of DNA diseases. Subsequently, different synthesis methods of MNCs are introduced. In the following section, DNA sensors based on different types of MNCs and their respective detection mechanisms are discussed in detail. Finally, the opportunities and challenges faced by DNA sensors based on MNCs are analyzed.

Keywords: biosensor; DNA probe; metal nanocluster; fluorescence; DNA hybridization

1. Introduction

After decades of development, nanomaterials are still a research area of wide concern [1]. Metal at the nanoscale can be categorized into metal nanoparticles and metal nanoclusters (MNCs) based on size regimes [2,3]. Atomically accurate nanoclusters (NCs) have different physical and chemical properties from nanoparticles (NPs) and are attracting more and more attention in different application fields, which further expands the vision of nanomaterial science. MNCs usually consist of tens to hundreds of atoms, with a core size of less than 2 nm, which is close to the Fermi wavelength of electrons, placing them between individual metal atoms and metal NPs [4–8]. The pronounced quantum confinement effect in MNCs leads to the division of continuous energy states into discrete ones. Their ultra-small size and discrete energy levels give rise to strong photoluminescence, redox capabilities, HOMO-LOMO transitions, large Stokes' shift, molecular magnetism, and other unique physical and chemical properties [5,9–12]. These features make MNCs promising in various applications like cancer treatment [13], antimicrobial therapy [14], imaging and sensors [15]. Among the features, their fluorescence property is particularly attractive, providing a pathway for high-performance sensors, imaging agents, photosensitizers and more. Sensors based on MNCs have been widely used in biomedical detection.

MNC-based sensors can be used to detect biological molecules such as deoxyribonucleic acids (DNAs), microRNAs, and proteins. As important biological macromolecules, DNAs are not only associated with the biological inheritance and the transmission of genetic information [16–18], but also with the occurrence of many diseases [19,20]. For example, single KRAS G12D-activated mutations often result in colorectal carcinoma [21]; HPV-16 DNA is associated with the heightened risk of cervical cancer [22]; CYFRA21-1 serves as an important marker for detecting lung cancers [23]. Therefore, the early and accurate detection

of DNAs is of great significance in healthcare. Although traditional detection methods such as DNA polymerase chain reaction (PCR) [24,25], enzyme-linked immunosorbent assay [26], and microarray analysis [27] are known for their high reliability, here are some disadvantages linked to them, such as high cost, complex operation, and high requirements for sample quality. DNA biosensors possess advantages such as ease of use, low cost, miniaturization, high sensitivity, and effectiveness [28,29]. New DNA detection methods include electrochemical sensing [30,31], surface plasma resonance, surface-enhanced Raman scattering, fluorescence and colorimetric sensing and so forth [32–34]. High sensitivity, selectivity, and rapid responsiveness are important parameters for sensors. The characteristics of MNCs offer significant advantages in optimizing these parameters [10,35–37]. Compared with traditional biosensors (such as quantum dots and organic dyes), MNCs possess characteristics such as strong light absorption and emission properties, good photostability, and biocompatibility. Moreover, by precisely controlling the size, shape, and composition of MNCs, the optical, electrical, and magnetic properties of MNCs can be regulated, thereby enhancing their interaction with DNA molecules and improving signal transduction, which greatly enhances the detection sensitivity and accuracy of biosensors [38]. Therefore, MNC-based sensors are a good option for the early and accurate detection of DNA.

This review focuses on MNCs that can be used in the early detection of DNA diseases. Firstly, various synthesis methods for MNCs, such as chemical reduction, ligand exchange, chemical etching, and other methods are introduced. In the following section, DNA sensors based on gold nanocluters (AuNCs), silver nanocluters (AgNCs), copper nanocluters (CuNCs) and bimetallic nanocluters, as well as corresponding detection mechanisms, are discussed in detail. Finally, the challenges in sensor development and potential solutions are addressed. This review aims to serve as a valuable resource for the design of future MNC-based DNA detection sensors and to inspire further research and innovation in MNC-based luminescent sensors.

2. Synthesis of Metal Nanoclusters

The great interest in synthesizing MNCs stems from their remarkable and diverse applications across various fields of modern science [9,39,40]. Therefore, numerous chemical and physical methods have been developed for the synthesis of MNCs with precise atomic compositions [41]. Up to now, atomically precise MNCs can be easily prepared through different synthesis methods [42,43]. As shown in Table 1, those methods include chemical reduction (Figure 1a), ligand exchange (Figure 1b), chemical etching (Figure 1c), and so on. For the early detection of DNA, MNCs with proteins or DNAs serving as ligands are typically synthesized.

Table 1. Comparison of the yield, reproducibility and scalability of different synthesis methods for MNCs.

| Synthesis Method of MNCs	Yield	Scalability	Reproducibility
Chemical reduction	Regulated by reactant concentration, reducing agent, temperature, and time	Higher	Higher
Ligand exchange	Governed by equilibrium constant, ligand concentration, and reaction activity	Low	Low
Chemical etching	Depends on material surface area, etchant concentration, and etching time	Medium	Medium
Microwave-assisted and green synthesis techniques	Influenced by microwave power, radiation time, reactant concentration, green solvents, and biocatalysts	High	High
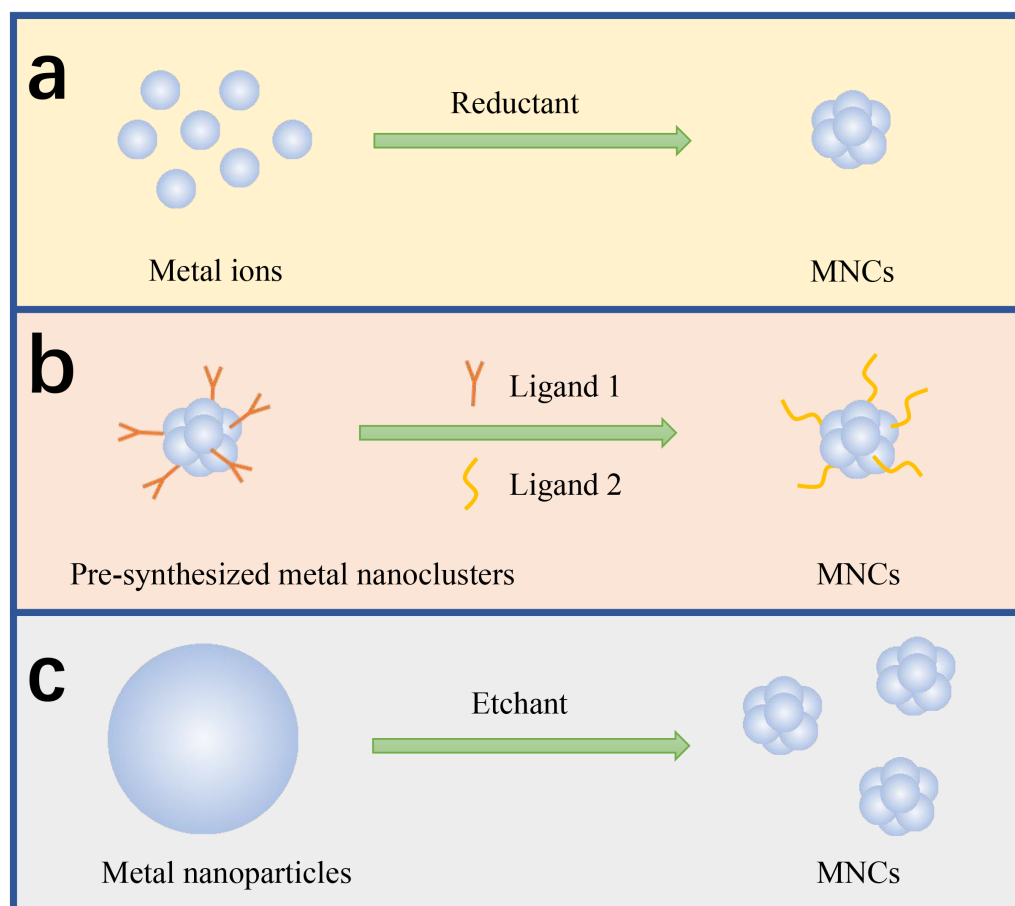
Figure 1. Schematic illustration of synthetic methods for MNCs: (**a**) chemical reduction; (**b**) ligand exchange; (**c**) chemical etching.

2.1. Chemical Reduction

As the most used method, chemical reduction is a "bottom-up" synthetic strategy. In a typical process, metal ions are reduced to lower-valent-state atoms in solution, followed by clustering them to form MNCs [44]. Reducing agents include Sodium Borohydride (NaBH$_4$), ascorbic acid, glutathione (GSH), etc. The reducing agent NaBH$_4$ can enhance the fluorescence quantum yield; the fluorescence emission wavelength of MNCs coated with the reducing agent GSH may shift; the reducing agent ascorbic acid can maintain the photophysical properties of MNCs. The speed of the reduction process and the strength of the reducing agent are crucial to the success of the reaction. The method is straightforward and rapid, and it can be conducted under mild conditions.

In the chemical reduction synthesis of MNCs, the most commonly used reducing agent is NaBH$_4$, which has mild reduction conditions. Zeng et al. reported the synthesis of the most stable medium-sized Au$_{64}$(S$-$c-C$_6$H$_{11}$) with a molecular weight of less than 20 kDa using NaBH$_4$ as a reducing agent [45]. The synthetic process consists of two parts. In the first part, Au(III) is converted to Au(I) via cyclohexanethiol, forming Au(I)S$-$c-C$_6$H$_{11}$ complexes, and the strong reducing agent NaBH$_4$ is added to further reduce Au(I) to Au(0). The coarse Au$_m$(S$-$c-C$_6$H$_{11}$)$_n$ clusters can be thereby obtained. In the second part, the crude product is dissolved in toluene and cyclohexanethiol, and it is gently stirred at 90 °C to obtain single-size Au$_{64}$(S$-$c-C$_6$H$_{11}$)$_{32}$ clusters. Chen et al. also used NaBH$_4$ as a reducing agent to develop a simple, gentle and rapid method for synthesizing well-dispersed AuAgNCs [46]. Firstly, HAuCl$_4$ was added to ultrapure water and mixed with AgNO$_3$ to form a flocculent precipitation. Next, GSH and NaBH$_4$ was added to the mixture in icy water. Finally, NaOH was added to adjust the pH to 7.5. The GSH@AuAgNCs

could be formed within 15 min at room temperature. Nasirian and coworkers reported that DNA-stabilized AgNCs could be prepared by mixing DNA, $AgNO_3$, $NaBH_4$ at an optimal molar ratio of 1:18:18 [47]. The synthetic reaction took 6 h in the dark environment.

Ascorbic acid, as a reducing agent, is often used to synthesize CuNCs. For example, a facile method to prepare water-soluble fluorescent CuNCs templated by nucleosides was reported [48]. In the synthesis, ascorbic acid was used as the reducing agent and nucleosides as stabilizers. During the formation of CuNCs, Cu(II) in copper nitrate were reduced to copper atoms by ascorbic acid, and then agglomerated to form CuNCs at 80 °C. At the same time, nucleotides comprised CuNCs to improve stability. Under neutral conditions, Tiwari et al., using adenine and thymine as templates, highly stable and highly fluorescent CuNCs with a very unique negative CD peak of about 350 nm were synthesized for the first time [49]. During the synthesis process, CuNCs exhibiting maximum fluorescence were synthesized by utilizing an optimal concentration of the reducing agent ascorbate at 2 mM and the optimal combination of DNA/Cu^{2+}/ascorbate at a ratio of 1:1000:400.

In addition to the above two, GSH has also been reported as a reducing agent in the chemical reduction synthesis of MNCs, and it can also act as a ligand. In 2018, Katla et al. reported a method for the rapid synthesis of AuNCs with excellent photothermal activity within 2 h without low-temperature conditions and agitation [50]. L-GSH was added to the $HAuCl_4$ solution, reducing Au(III) to Au(I). To this mixture, $NaBH_4$ was added to further reduce Au(I) to Au(0). Finally, methanol was added to precipitate AuNCs, which were obtained by centrifugation and by removing the supernatants. Yan et al. successfully synthesized stable CuNCs by utilizing GSH as both a reducing agent and protecting agent [51]. The turbid liquid mixture of $CuCl_2$ and GSH was clarified with NaOH and then stirred at 80 °C for 24 h to yield CuNCs, which can be further utilized after being washed with isopropyl alcohol multiple times.

2.2. Ligand Exchange

The ligand exchange method allows selective replacement of the surface ligands of MNCs to produce new MNCs [52,53]. This method can impact the core size, geometry, solubility, and photoelectric properties of MNCs significantly. The ligand exchange reaction can control the size of MNCs through a fast and direct process.

Liu and coworkers reported that $Au_{144}(SCH_2Ph)_{60}$NCs were obtained from polydispersed $Au_n (SG)_m$NCs in the presence of excess phenyl methanethiol ($H-SCH_2PH$) ligands via multiple "ligand exchange" processes [54]. Toluene, ethanol and $H-SCH_2PH$ were added to $Au_n (SG)_m$NCs, and $Au_n (SCH_2PH)_m$NCs were prepared by the exchange of ligand $(SG)_m^{n-}$ and $(SCH_2PH)_m^{n-}$. Shichibu and coworkers reported a large-scale synthesis of thiolate-capped Au_{25} clusters via a ligand exchange reaction with phosphine-stabilized Au_{11} clusters [55]. Meanwhile, they found that thermodynamically stable $Au_{25}(SG)_{18}$ can be selectively obtained on the sub 100 mg scale under controlled conditions. Various ligands have been used to synthesize AgNCs, including DNA [56], thiolates [57], polymers [58], peptides [59], and proteins [60]. Chang et al. conducted a ligand exchange reaction, replacing the ligands of $Ag_{21}[S_2P(OiPr)_2]_{12}$ with $NH_4[Se_2P(OEt)_2]$ to produce $Ag_{21}[Se_2P(OEt)_2]_{12}$ clusters [61]. Bootharajuet et al. reported the interconversion between $Ag_{25}(SPhMe_2)_{18}$NCs and $Ag_{44}(SPhtF)_{30}$NCs. Exchanging the ligands of non-hollow $Ag_{25}(SPhMe_2)_{18}$ with excess HSPhtF ligands yielded hollow $Ag_{44}(SPhtF)_{30}$NCs [62].

Compared with AuNCs and AgNCs, the ligand exchange method is relatively less used in the synthesis of CuNCs, but there are some related reports. Nguyen et al. reported the synthesis of novel Cu_{29}NCs based on the cluster growth initiated by the ligand exchange reaction [63]. In the synthetic process, the ligand exchange reaction produces $CuCl_2$

monomers, which are then captured by $Cu_{25}NCs$ to generate $Cu_{29}NCs$. $Cu_{29}NCs$ are the largest copper superatoms known to date.

2.3. Chemical Etching

Chemical etching is achieved by etching large NPs into small NCs, which is a "top-down" synthetic strategy [64,65]. MNCs can be obtained by etching metal nanoparticles using different etching agents.

At present, the etch agents reported include GSH, H_2O_2, cysteamine hydrochloride, and ammonia. Then, a series of descriptions are given on the synthesis of MNCs using these etchers. Le Guével's group converted silver nanoparticles to non-bleaching and highly photostable AgNCs via GSH as the ligand etchant [66]. By changing the reaction time with the etchant (one day, three days, and eight days), the samples were washed several times with acetone, and AgNCs with red, blue and yellow fluorescence were obtained, respectively. Chen and coworkers reported a facile, simple and rapid chemical etching method for preparing AuNCs capped with luminol at room temperature [67]. Firstly, AuNCs were synthesized by a mixed solution of $HAuCl_4$ and luminol, and then the GSH etchant was added to obtain green-fluorescent AuNCs.

Liu et al. found that etching AgNCs with H_2O_2 led to the formation of smaller clusters, increasing the fluorescence intensity of GSH-AgNCs [68]. In the study by Shen et al., bovine serum albumin stabilized gold nanoparticles (AuNPs) were obtained by a typical reduction method [69]. Then, a solution comprising AuNPs was mixed with the etchant, cysteamine hydrochloride, at a volume ratio of 1:3, to etch AuNPs to form AuNCs. Deng's group reported that the conversion of non-luminescent copper NPs to luminescent CuNCs was achieved by using ammonia as the etchant [70]. The etching process using ammonia gas is rapid, taking 15 min, and yields CuNCs with strong green fluorescence.

2.4. Other Synthetic Methods

Microwave-assisted and green synthesis technologies are becoming increasingly important in the field of MNCs synthesis, not only by helping to improve synthesis efficiency and reduce costs but also by having a lesser impact on the environment, thus facilitating the achievement of more sustainable and cost-effective synthesis methods. For example, Saleh and colleagues developed a microwave-assisted synthesis method, which is fast and environmentally friendly. In this method, the pepsin molecule is used as a stabilizer and reductant. The mixture of copper nitrate, pepsin and sodium hydroxide is irradiated in a microwave oven for 30 min, and then the microwave-assisted solution is dialyzed overnight in ultrapure water to obtain pepsin CuNCs. There are some synthesis methods that use ultrasound or microwave, and the whole process does not use any additional reducing agent [71]. Sadhu and coworkers reported a facile, microwave method to fabricate blue-fluorescent CuNCs from the extract of *Bacopa monnieri* [72]. Li et al. used poly metacrylicacid, sodium saltas on the surface ligand to synthesize water-soluble fluorescent AgNCs by microwave radiation [73]. This method is fast, simple, and highly repeatable. For the first time, Naaz's team has synthesized AgNCs with photoluminescence through fine tuning of sunlight and ultrasound [74]. A more convenient method was also mentioned, and Zhang et al. reported the synthesis of natural silk fibroin-stabilized CuNCs by a one-pot method, which has excellent water solubility and pH responsiveness [75]. The sensor based on it has a fast response and a wide detection range.

3. MNCs for DNA Detection

This section discusses different MNC-based sensors for DNA detection. DNA, a biological macromolecule with good biocompatibility and water solubility, serves as the most commonly used template for MNCs [76]. DNA-templated MNCs have shown great potential in biochemical sensing, including DNA detection [77–79]. Besides DNA, proteins are also effective templates for MNCs used in DNA detection [80,81]. This section introduces four types of MNCs, namely AuNCs, AgNCs, CuNCs, and alloy NCs, as DNA sensors.

3.1. AgNCs for DNA Detection

AgNCs have been at the forefront of research due to their ease of synthesis, good photostability, and the lower cost compared to their gold counterparts. AgNCs are mainly used in biological sensing [82,83]. Among all the AgNCs, DNA-templated AgNCs exhibit the most excellent physical and chemical properties [4], in terms of quantum yield, photostability, redox, emission tunability and very high specific surface product properties [84,85]. The properties of MNCs are largely influenced by the design of DNA templates. For example, DNA template AgNCs (DNA-AgNCs) can display bright light tunable emission colors and enhance stability by adjusting the sequence of the DNA template. Therefore, DNA-AgNCs are promising sensors for DNA.

High fluorescence performance is critical for accurate DNA detection. Compared with optical quantum dots-QDs and organic dyes, DNA-AgNCs have the advantages of a long fluorescence period and low toxicity [84,86,87]. DNA-AgNCs typically show high sensitivity in DNA detection, allowing AgNC-based sensors to accurately detect DNA without the need for amplification methods. DNA hybridization technology utilizes the complementary pairing between DNA strands to achieve specific recognition of target DNA. The direct hybridization of DNA templates enables highly selective sensing of targets, leading to the development of many sensing platforms [88] (Figure 2a). For instance, Lee et al. discovered that guanine-rich-DNA-AgNCs show highly selective responses to FOXP3 DNA [89], with a limit detection reaching as low as 0.625 µM. The hybridization of AgNCs with a guanine-rich chain and target DNA will produce a three-way target sequence, which will shift the fluorescence spectrum and increase the fluorescence intensity. Changes in fluorescence intensity allow for the quantitative detection of FOXP3 DNA. Zhou et al. used A_{20}-C55 DNA-AgNCs as the fluorescence probes of the ratio fluorescence sensor [90]. The probe has good sensitivity, versatility, a high signal-to-noise ratio, etc. When there is no target DNA, it presents a single yellow fluorescence emission at 570 nm. When it hybridizes with target DNA and approaches non-fluorescent auxiliary AgNCs, the yellow fluorescence emission signal decreases, while a new red emission signal increases. In this way, a controllable fluorescence color transition from yellow to red is achieved, offering a suitable platform for analyzing HBV and HIV.
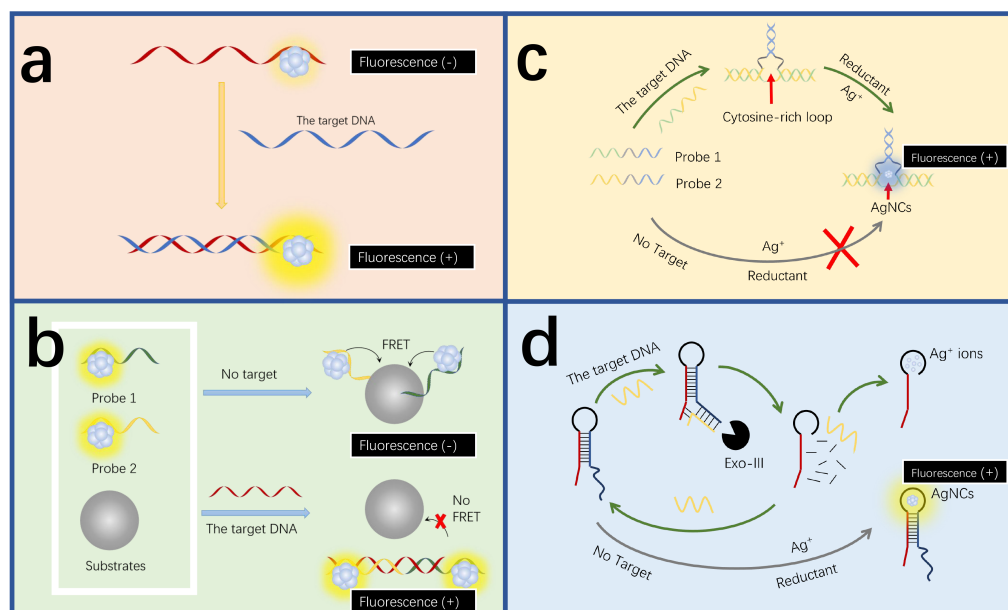
Figure 2. DNA detection mechanisms of fluorescent AgNC-based sensors. (**a**) Direct hybridization-induced fluorescence quenching. The target hybridizes with the DNA-AgNCs to directly change the fluorescence intensity. Redrawn from [89]. (**b**) Indirect hybridization-induced fluorescence quenching. The target hybridizes with the DNA-AgNCs to indirectly change the fluorescence intensity, for example, by disrupting the resonance energy transfer process. Redrawn from [91]. (**c**) The fluorescence quenching by the interaction between sequence bases and AgNCs. The target induces the formation of cytosine-rich structures, favoring the generation of fluorescent AgNCs and thereby increasing the fluorescence intensity. Redrawn from [92]. (**d**) Amplification strategy-assisted DNA detection. The schematic diagram of the label-free assay for enzymatic amplification DNA detection. Redrawn from [93].

In addition to the direct hybridization strategy, indirect hybridization is another common approach for DNA detection using DNA-AgNCs (Figure 2b). There is also a fluorescence detection strategy that utilizes fluorescence resonance energy transfer (FRET) between dyes and nanomaterials to analyze the object [94,95]. A sensing platform based on carbon nanoparticle (CNP) oxide and DNA functionalization of AgNCs was prepared [91]. The fluorescence resonance energy transfer between AgNCs and CNPs oxide was mainly used to detect HIV-DNA. When the target DNA is absent, the two capture probes after functionalization of AgNCs are adsorbed to CNPs oxide, resulting in the emission of AgNCs being quenched. When the target DNA is present, the two capture probes after AgNCs functionalization hybridize with the target HIV-DNA to form dsDNA. Due to the weak adsorption of dsDNA by CNPs oxide, the two capture probes are far away from the CNPs oxide, resulting in AgNCs emitting light. The sensor can be used to detect single base mismatch and has strong specificity.

The interaction between DNA templates and AgNCs can be also utilized for DNA detection (Figure 2c). The intensity of DNA-AgNCs can be affected by the base sequences of the DNA templates [96]. For example, the high affinity of silver ions with cytosine (C) groups can further promote the formation of AgNCs in situ [97,98]. Guanine (G) can enhance the fluorescence intensity of AgNCs [99]. Based on this feature, Zhang and colleagues developed a labeling-free fluorescence sensing platform based on three-segment-branched DNA-AgNCs [92]. When H5N1 virus DNA is present, complementary base pairing occurs between the probe and H5N1 to form a closed cytosine-rich loop that can chelate Ag^+ to generate AgNCs. The target gene can be qualitatively and quantitatively detected according to the change of fluorescence intensity. The sensor has a wide linear detection range of 500 pM–2 nM. Zou et al. built up a high-sensitivity detection platform

using AgNCs for HIV-1 and HIV-2. The platform is based on fluorescence enhancement of guanine-rich sequence and AgNCs dimerization [100]. When the target DNA is missing, the fluorescence signal at one end of the AgNCs is enhanced due to the presence of a G-rich sequence, while the signal at the other end is enhanced due to the interaction between the two AgNCs. The hybridization of the target DNA with the probe separated the G-rich sequence from the AgNCs. At the same time, it depolymerized the dimerized AgNCs. The fluorescence intensities of the AgNCs at both ends were weakened. This multi-channel analysis platform for the target DNA exhibits high selectivity and a low detection limit of 11 pM.

Early detection of DNA requires sensors to be ultrasensitive. DNA amplification strategies can significantly enhance the sensitivity of sensors by amplifying DNA signals. To date, major multiple amplification strategies for DNA detection include enzyme-free and nuclease-based strategies [101–103]. A typical example of enzyme-free amplification is the hybridization chain reaction (HCR) strategy. HCR is an isothermal and enzyme-free process in which the cascade reaction is initiated by the target analyte [88,104,105]. Due to its advantages, such as the autonomous isothermal replication process, high enzyme-free amplification efficiency and controllable kinetics, biosensors based on HCR for DNA detection have been reported [106,107]. Wong and colleagues report a DNA biosensor based on HCR and AgNCs with a detection limit of 3.35 fM [108]. In the absence of DNA-214, the hairpin structures (H1 and H2) do not trigger HCR, and the addition of P1 (the sequence region rich in cytosine) can form a relatively stable P1-H1 double-stranded structure, in which the AgNCs on P2 (the core sequences) remain non-fluorescent. When the target DNA is present, H1 and H2 participate in the amplification process of the HCR, which causes the hybridization of P1 and P2 and generates the emission of red fluorescence. This is because the P1-P2-AgNCs complex promotes the end-to-end transfer of non-fluorescent AgNCs from the P2 end to the cytosine-rich region of P1 and then activates the red-emitting substances. The intensity of this red fluorescence increases as the concentration of the target DNA rises. Chen et al. used the formation of cytosine-rich sequences to promote the in situ generation of AgNCs and developed an autocatalytic strand displacement amplification with continuous HCR for effective coupling of DNA biosensors [109]. In the presence of target DNA, this strategy causes displacement amplification of the autocatalytic chain, generating many identical auxiliary DNA strands (ASs) corresponding to the target DNA within the DNA fragments. These can be used for further hybrid identification and amplification processes. The ASs from the ASDA chain can be used as primers, and they can propagate the HCR between two hairpins (H1 and H2), forming a series rich in cytosine that can promote the in situ generation of AgNCs. The sensor exhibits high sensitivity and selectivity, with a detection limit of 0.16 fM.

Signal amplification based on nuclease includes stand displacement amplification and Exonuclease-III(Exo-III)-assisted amplification (Figure 2d). Exo-III-assisted strategies, in which Exo-III is a sequence-independent enzyme that catalyzes the gradual removal of 3′ hydroxy-terminal single nucleotides [110–112], provide a universal platform for DNA detection. The strand displacement amplification method involves polymerase extension and endonuclide cleavage, offering an amplification efficiency up to 10^7. The strategy is characterized by its homogeneity and label-free nature [113]. Yang and colleagues successfully constructed a fluorescent biosensor platform based on a probe for spherical recognition and a AgNC-based switch initiated by the strand displacement reaction [114]. The sensor has a detection limit of 250 pM, with a good recovery ability. When the target DNA associated with Alzheimer's disease is present, the capture probe on the surface of the magnetic bead hybridizes with it, forming a blunt 3′ end that further activates the Exo-III enzyme, resulting in the release of the target DNA and the trigger chain. The trigger chain

leads to the chain shift reaction, sharply decreasing the fluorescence intensity of AgNCs. While the absence of the target will neither activate the Exo III enzyme nor release the trigger chain, intense red fluorescence can be observed as a result. Shen et al. developed a label-free and visual probe for DNA detection using the hairpin-templated AgNCs [93]. When the target DNA is absent, the hairpin DNA probe leads to the in situ formation of highly fluorescent AgNCs. When the probe recognizes the target DNA, it forms a three-way junction structure. Exo-III gradually degrades the three-way junction structure, destroying the hairpin DNA probe and reducing the amount of highly fluorescent AgNCs. Therefore, the fluorescence intensity is inversely proportional to the target concentration.

The silver nanocluster beacons (AgNCBs) are label-free, activated fluorescent probes with a core consisting of few-atom AgNCs [115]. AgNCBs offer various modalities of responses, including "turn-on" and "chameleon" mechanisms, and they do not rely on FRET for their activation or color change [116]. In comparison to AgNCs, AgNCBs show advantages in target recognition, ease in activation, and exhibit greater resistance to enzymatic degradation [117].

Most reported AgNCB-based sensors employ a single-emission on/off signal readout strategy, which is limited by sensing interference from environmental and/or experimental conditions. However, the proportional fluorescence biosensor based on AgNCBs can simultaneously record the relative fluorescence changes of two well-separated wavelengths, which can further improve the sensitivity and accuracy of biosensing by eliminating systematic errors and can more accurately quantify the target concentration [118–120]. The "chameleon" in NCBs shows that when the converter is close to DNA-AgNCs, a more resolved multicolor fluorescence signal can be obtained, usually using the ratio of fluorescence intensity as the output signal.

AgNCBs are commonly used as a fluorescence ratiometric sensor, detecting DNA by fluorescence emission wavelength more than intensity. The fluorescence detection mechanism based on AgNCB is unique to AgNCs. In Ge et al.'s study, a fluorescence ratio biosensing platform was developed for detecting Werner syndrome (WS)-related DNA using a catalytic hairpin assembly expansion strategy based on AgNCBs [118]. Ratiometric catalyzed-assembly AgNCBs can detect target DNA by converting green-emitting AgNCs into red AgNCs when they are near a particular DNA fragment (Figure 3a). With a detection limit of 8.5 pM and a wide linear detection range, the sensor is suitable for detecting WS -related gene targets in human serum. Ge et al. developed a DNA fluorescence ratio sensor fort Hepatitis-A (HAV) based on AgNCBs [119]. In this sensor, the fluorescence color transition from red to green indicates whether the specific DNA fragment is linked to the green nucleation sequence (GNuS) of AgNCs. The presence of target DNA disrupts the hairpin structure of NCBs, physically separating the special DNA fragment from GNuS and resulting in a green emission. While in the absence of target DNA, the hairpin structure of NCBs remains intact, keeping the converter and GNuS connected and generating a red emission.

AgNCBs can also be used for dual DNA detection, which can avoid false diagnoses and overcome the time-consuming drawback observed in traditional methods [121]. Feng et al. developed a sensing platform for the simultaneous detection of H1N1 and HIN5 DNA of influenza viruses (Figure 3b), which is capable of identifying subtype genes within the same virus [117]. The sensor is constructed using AgNCBs and AuNPs, where there are two types of AgNCBs responding to two different DNA targets, realizing a dual detection. When there is no target, the fluorescence is quenched by the energy transfer between AuNPs and AuNCs. In the presence of the target DNA, the hairpin-structure AgNCBs transform into rigid double-stranded (dsDNA), separating AuNPs and AuNCs, disrupting the energy

transfer and increasing the fluorescence intensity. Therefore, the notable fluorescence signals reflect the presence of DNA targets.

Figure 3. (**a**) The schematic of ratio-fluorescent biosensing platform based on RCA-amplified AgNCBs. Reproduced with permission from [118]. Copyright 2017 American Chemical Society. (**b**) Schematic illustration of dual DNA sensors based on AgNCBs and AuNPs. Reproduced with permission from [117]. Copyright 2023 Elsevier.

Currently, AgNCB-based sensors are not only used for detecting multiple DNA targets from viruses but also for sensing multiple analytes, including DNA, small molecules and proteins. Liu et al. successfully synthesized activated AgNCBs using a well-designed multifunctional single-stranded DNA sequence [122], which comprises a segment capable of forming AgNCs, a target recognition segment, and a segment used for attaching quenching agents. The sensor works on the FRET mechanism, where the interaction with the target molecule disrupts the beacon's hairpin structure, leading to detachment from the quencher and a consequent rise in fluorescence. By varying the design of the target recognition sequence, this sensor facilitates the detection of multiple DNA sequences, small molecules, and proteins.

In this chapter, DNA detection sensors based on AgNCs are categorized into two major groups: those based on AgNCs and those based on AgNCBs. The data presented above indicate that silver ions exhibit a strong affinity for cytosine, and DNA sequences rich in cytosine significantly facilitate the formation of AgNCs. Reactions such as strand

displacement, HCR and Exo-III-assisted amplification are employed to amplify the detection signal, thereby achieving a low detection limit. Table 2 reveals that the minimum detection limit can reach the pM level, exhibiting a high sensitivity.

Table 2. Recently reported MNCs for DNA detection.

Material	Synthesis Template	Detecting Technology	Target	Detection Limit (M)	Linear Range (M)	Ref.
AgNCs	DNA	Fluorescence	FOXP3-DNA	6.25×10^{-7}	-	[89]
AgNCs	DNA	Ratiometric fluorescence	HIV-DNA HBV-DNA	5×10^{-9}	5×10^{-9}–10×10^{-7}	[90]
AgNCs	-	Fluorescence	HIV-DNA	4×10^{-8}	1×10^{-9}–5×10^{-8}	[91]
AgNCs	-	Fluorescence	H5N1-DNA	5×10^{-10}	5×10^{-10}–2×10^{-9}	[92]
AgNCs	DNA	Fluorescence	two HIV DNA	1.2×10^{-11}	2×10^{-8}–7×10^{-8}	[100]
AgNCs	DNA	Fluorescence	DNA-214	3.35×10^{-15}	0–1×10^{-9}	[108]
AgNCs	DNA	Electrochemistry	-	1.6×10^{-16}	1×10^{-11}–2.5×10^{-8}	[109]
AgNCs	DNA	Fluorescence	Alzheimer disease DNA	2.5×10^{-10}	2.5×10^{-10}–2.5×10^{-8}	[114]
AgNCs	DNA	Fluorescence	-	2.8×10^{-9}	5×10^{-9}–5×10^{-8}	[93]
AgNCBs	DNA	Fluorescence	H1N1-DNA H5N1-DNA	1×10^{-11}	1×10^{-12}–2×10^{-10}	[117]
AgNCBs	DNA	Ratiometric fluorescence	WS-DNA	8.5×10^{-12}	0–8×10^{-8}	[118]
AgNCBs	DNA	Ratiometric fluorescence	HAV-DNA	5×10^{-10}	1×10^{-9}–5×10^{-7}	[119]
AuNCs	hemoglobin	Electrochemistry	BCR/ABL-DNA	3.7×10^{-17}	1×10^{-14}–1×10^{-12}	[123]
AuNCs	graphene	Electrochemistry	-	5.7×10^{-17}	2×10^{-14}–2×10^{-12}	[124]
AuNCs	graphene	Electrochemistry	HIV-DNA	3×10^{-17}	1×10^{-16}–1×10^{-14}	[125]
AuNCs	avidin	Fluorescence	-	4.3×10^{-11}	2×10^{-10}–2×10^{-8}	[126]
AuNCs	DNA	Fluorescence	H1N1-DNA	2×10^{-10}	1×10^{-10}–1×10^{-8}	[127]
AuNCs	-	Electrochemiluminescence	HPV16 E7-DNA	6.8×10^{-18}	1×10^{-16}–1×10^{-14}	[128]
AuNCs	-	Electrochemiluminescence	HPV-16DNA	4.8×10^{-13}	1×10^{-12}–1×10^{-10}	[129]
AuNCs	L-methionine	Surface-enhanced Raman spectroscopy	ctDNA	4.24×10^{-15}	0–1×10^{-12}	[130]
CuNCs	DNA	Fluorescence	-	1×10^{-12}	5×10^{-12}–5×10^{-11}	[131]
CuNCs	DNA	Ratiometric fluorescence	HTLV-1	1×10^{-11}	2×10^{-11}–1.2×10^{-9}	[132]
CuNCs	DNA	Fluorescence	HBV-DNA	5.4×10^{-13}	5×10^{-12}–1×10^{-10}	[133]
CuNCs	DNA	Fluorescence	C.trachomatis DNA	1.85×10^{-8}	5×10^{-8}–1×9.5^{-7}	[134]
CuNCs	DNA	Fluorescence	BRCA1-DNA	2×10^{-9}	2×10^{-9}–6×10^{-7}	[135]
Au/AgNCs	DNA	Fluorescence	campylobacter jejuni-DNA	4.4×10^{-12}	1×10^{-11}–3×10^{-9}	[136]
Au/Ag/PtNCs	DNA	Electrochemistry	β-thalassemia-DNA	8×10^{-16}	1×10^{-15}–1×10^{-13}	[137]
Ag/PtNCs	-	Field-effect transistor	-	1.28×10^{-9}	-	[138]

3.2. AuNCs for DNA Detection

AuNCs emerge as increasingly popular DNA sensors [139,140], due to their superior biocompatibility and stability [141–145]. DNA and protein-templated AuNCs stand out as the most commonly used ones for DNA detection, among all the AuNCs capped by different ligands, like thiols [146], polymers [147], DNA [148], peptides [149], and proteins [150].

Electrochemical sensing is widely used in DNA detection for its advantages of high sensitivity, fast response and low cost [151–154] (Figure 4a). Shamsipur et al. developed an electrochemical sensor for BCR/ABL fusion genes based on graphenes covered by hemoglobin-templated AuNCs [123]. When the complementary DNA hybridizes with the probe ssDNA, methylene blue in the probe ssDNA is released upon interaction with the complementary DNA, reducing the differential voltammetry current and increasing the electrochemical impedance spectroscopy resistance. The detection limit of the sensor is 0.037 fM. Wang and colleagues pioneered the integration of AuNCs/graphene (GR) nanocomposites with an Exo-III-mediated target recycling strategy to fabricate an electrochemical DNA sensor [124]. The target DNA initiates the Exo-III cascade target cycle process, producing cleavage products that facilitate the connection between the capture probe and AuNCs/GR-DNA-alkaline phosphatase, which is anchored on the electrode. AuNCs/GR-DNA-alkaline phosphatase further catalyzes the deposition of silver to form AgNPs on the electrode, generating electrical signals that are used for the quantitative DNA detection, with a detection limit of 0.057 fM. Wang et al. developed an HIV-DNA electrochemical biosensor based on graphene-stabilized AuNCs (GR/AuNCs) [125]. The glassy carbon electrode modified by GR/AuNCs provides more fixed sites for the capture probe. The target DNA hybridizes with the capture probe to form a double-stranded DNA structure. This triggers the Exo-III enzyme to cleave the 3′ end of the capture probe,

releasing methylene blue molecules from the electrode surface and recovering the target DNA. This results in current changes, allowing for the quantitative detection of HIV-DNA, with a detection limit reaching 30 aM.
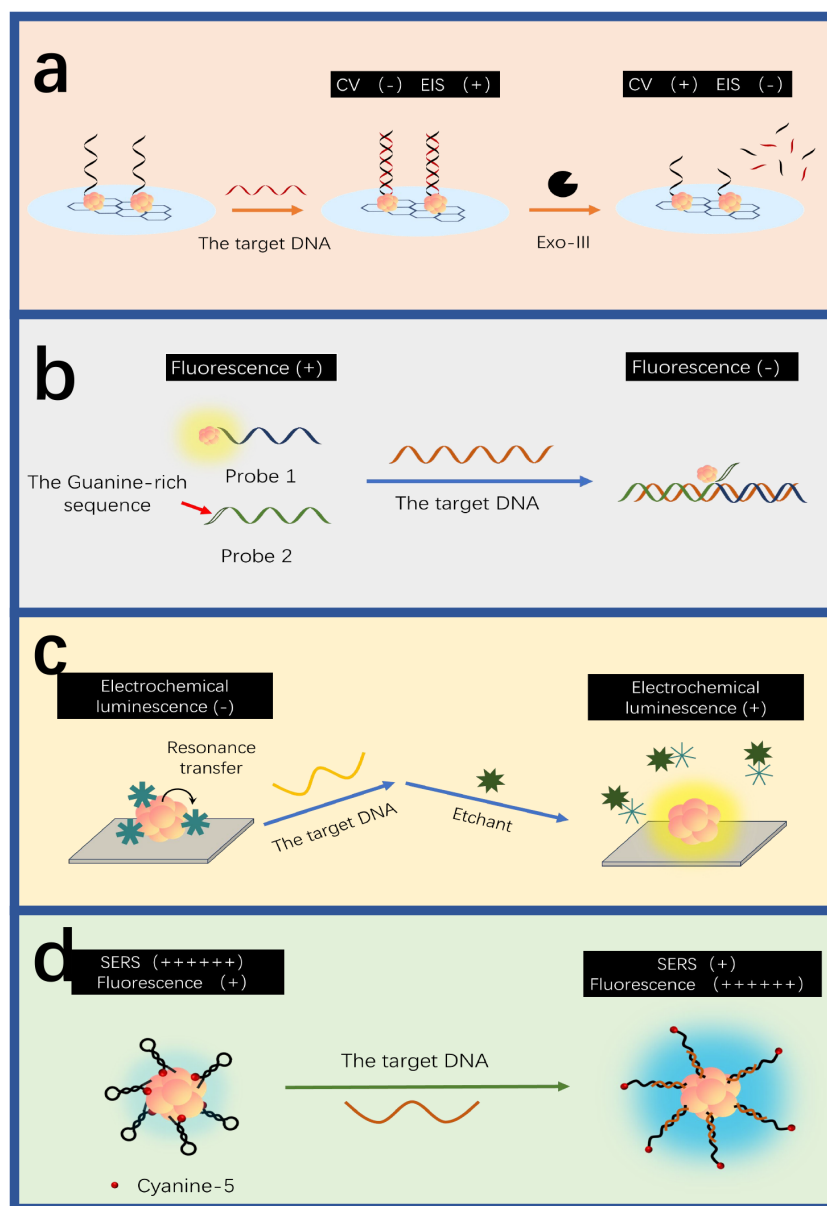

Figure 4. DNA detection mechanisms of AuNC-based sensors. (**a**) The electrochemical detection using Exo III-assisted target cycle amplification strategy. The hybridization between the target and DNA-AuNCs decreases the impedance. Redrawn from [124]. (**b**) The fluorescent detection. The hybridization among the target, the guanine-rich sequence and the DNA-AuNCs decrease the fluorescence intensity. Redrawn from [127]. (**c**) Electrochemical-luminescent detection. The target disrupts the resonance transfer between AuNCs and MnO_2, increasing the intensity of electrochemical luminescence. Redrawn from [128]. (**d**) The detection based on SERS. The target hybridizes with the hairpin DNA-AuNCs to yield strengthened SERS signals. Redrawn from [130].

AuNCs are known for their superior fluorescence properties, which can be utilized for sensitive, selective and quantitative DNA detection (Figure 4b). Tang et al. used avidin-stabilized AuNCs (Av-AuNCs) as a fluorescence sensor for DNA [126] (Figure 5). When the target DNA exists, it hybridizes with the capture DNA chain and the helper DNA, forming a sandwich structure. Subsequently, a linker chain modified with biotin at both ends is added to crosslink Av-AuNCs and magnetic beads, resulting in strong fluorescence signals.

Thus, the fluorescence intensity rises with the target concentration, and the linear detection range is 20 μM–0.2 nM. Unlike the fluorescence quenching mechanism of AgNCs based on Förster resonance energy transfer, the fluorescence quenching of AuNCs is mainly based on the mechanism of photoinduced electron transfer. Wang et al. developed a marker-free sensor for H1N1 DNA based on proximity-dependent hybridization and guanine-induced fluorescence quenching [127]. This fluorescent sensing platform has a detection limit of 200 pM. Upon hybridization of the target DNA with P2DNA—which includes a template sequence for the synthesis of AuNCs and hybridization sequences—and 6G probe 2—which comprises guanine-rich overhang sequences and hybridization sequences—a "Y"-shaped structure is formed. This configuration leads to substantial fluorescence quenching when in proximity to DNA-AuNCs and G-rich sequences, likely due to the photoinduced electron transfer between the AuNCs and the guanine-rich DNA. When there is no target, the 6G probe 2 emits strong fluorescence at 475 nm of excitation. The target concentration is inversely proportional to the fluorescence intensity.
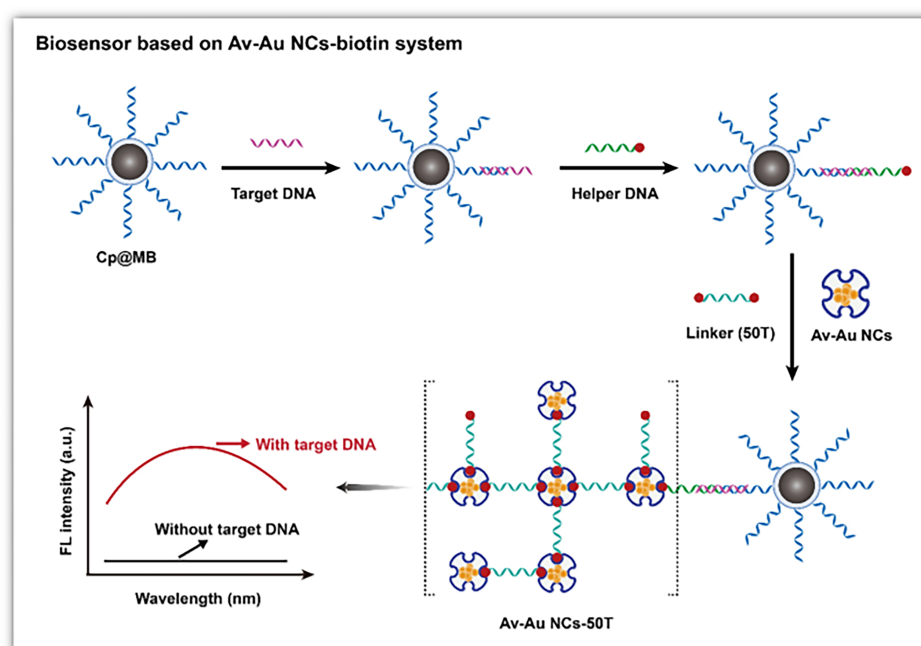
Figure 5. Schematic illustration of the fluorescent DNA biosensor based on the Av-AuNCs-biotin signal amplification system. Reproduced with permission from [126]. Copyright 2022 Springer.

In addition to electrochemical and fluorescent methods, electrochemical luminescence (ECL) is also considered as a powerful and promising technique for DNA detection due to its rapid responses, low background noises, and high sensitivity [155–158] (Figure 4c). Hong et al. designed an ECL sensor based on AuNCs to probe HPV-16 DNA, which has a detection limit of 6.8 aM [128]. In the absence of the target DNA, the ECL signal is weak due to the resonant transfer between AuNCs and manganese dioxide particles. However, when the target DNA is present, it hybridizes with the capture probe and the biotin probe to form a "sandwich" structure known as the biotinylated DNA complex. This triggers a reaction between streptin-alkaline phosphatase and the biotinylated DNA complex to produce ascorbic acid, which etches manganese dioxide particles to curb the resonant transfer between manganese dioxide particles and AuNCs, resulting in significant ECL signals. The concentration of the target DNA is thereby proportional to the intensity of ECL signals. Liu and colleagues developed an ECL biosensor using Clustered Regularly Interspaced Short Palindromic Repeats (CRISPR)-associated 12a for target amplification in the HIV-DNA testing [129]. Archaea and bacteria can be used for signal amplification

in the CRISPR/Cas system, which is widely used for the accurate diagnosis of nucleic acids [159,160]. The CRISPR/Cas system has a biological activity known as "genetic scissors", which can identify and cut the specific DNA target sequences upon the guidance of CRISPR RNA, further activating its cutting ability [161–164]. The sensor employed L-methionine-stabilized AuNCs (Met-AuNCs) as an efficient ECL emitter. Ferrocene-tagged thiolated single-strand DNA (SH-ssDNA-FC) was introduced to quench the Met-AuNCs launch, leading to weak ECL signals. When the target DNA was present, the nonspecific ssDNA trans-cutting ability of Cas12a was activated, resulting in the indiscriminate cutting of SH-ssDNA-FC. As a result, ECL signals were greatly recovered. The target DNA can be quantitatively determined by correlating ECL signals with different target concentrations.

Surface-enhanced Raman scattering (SERS) can sensitively identify patterns of biomarkers in a single spectrum without the need for complex array structures of sensors [165–170]. Guo et al. used asymmetric polymerase chain reaction (PCR) and SERS to detect EGFR mutations [130]. In the absence of the target DNA, when the molecular beacon was in a loop-stem structure, the SERS signals of AuNCs were strong. However, when the target was present, multiple target objects produced by PCR could hybridize with the molecular beacon, forming a double-helix structure and keeping 5′ Cy3 far away from AuNCs. This significantly reduces the SERS signal.

This part focuses on AuNC-based sensors that can detect DNA through various modalities, including electrochemical, fluorescent, ECL, and SERS methods. Most of these sensors utilize AuNCs template by DNA and proteins, with those integrated with CRISPR/Cas systems showing significantly improved sensitivity in detection. As shown in Table 1, the minimum detection limit can reach the aM level.

3.3. CuNCs for DNA Detection

DNA-templated CuNCs (DNA-CuNCs) emerge as promising DNA sensors with ease in preparation and relatively low cost [171,172], despite them not been as widely reported as AgNCs and AuNC-based sensors [75].

CuNCs can show better performance in DNA detection than AgNCs and AuNCs. Tao et al. developed a fluorescent sensor based on CRISPR-Cas12a enzyme and MNCs, including AuNCs, AgNCs and CuNCs, for the detection of hepatitis B virus (HBV)-DNA [133]. The presence of the target causes Cas12a to indiscriminately cut the DNA probe, inhibiting the formation of MNCs and thus decreasing the fluorescence intensity, which is inversely proportional to the target concentration. Compared with AuNCs and AgNCs, CuNCs show faster responses and higher sensitivity, reaching a response time of 25 min and a detection limit as low as 0.54 pM.

Different from AgNCs and AuNCs, the fluorescence detection of CuNCs is mainly based on the interaction between DNA bases and structures and CuNCs to achieve the detection of target DNA. The adenine and thymine-rich sequences serve as an effective template for highly fluorescent CuNCs [173,174] (Figure 6a). This feature can be utilized in indirect probing of DNA, where the target concentration is determined by the change in fluorescence intensity induced by the formation of CuNCs in adenine and thymine-rich DNA. For example, Chen et al. utilized this feature to construct a fluorescent sensor for lymphotropic virus DNA [132] (Figure 7). The sensor has a detection range of 20 pM–12 nM. When the target DNA is present, an amplification strategy using the EXO-III-assisted target recycling is adopted to produce a large amount of AT-rich single DNA(oDNA). The DNA1 on the graphene quantum dots (GQDs) can then hybridize with the oDNA to form GQDs-ss\sdsDNA, which is resistant to digestion because of the EXO-III. On the GQDs-sdsDNA, fluorescent CuNCs can be generated. The change in fluorescence intensity reveals the concentration of the target DNA. Similarly, Chen et al. developed a fluorescence sensor

for viral genetic DNA based on the in situ formation of fluorescent CuNCs from AT-rich double-stranded DNA [131]. The sensor uses target recycling amplification and magnetic separation strategies, with a detection limit as low as 1 pM. When the target DNA is present, a large number of DNA output regions (oDNA) are released after amplification of the target cycle. oDNA cannot only hybridize with the capture DNA, which is coupled on the surface of magnetic beads, but also with the AT-rich dsDNA in the solution, which is used for the formation of fluorescent CuNCs. The remaining dsDNA in the solution can be obtained by magnetic separation and used to form CuNCs. By correlating the fluorescent intensity of the as-formed CuNCs with the concentration of remaining dsDNA, the concentration of the target DNA can be thereby determined.
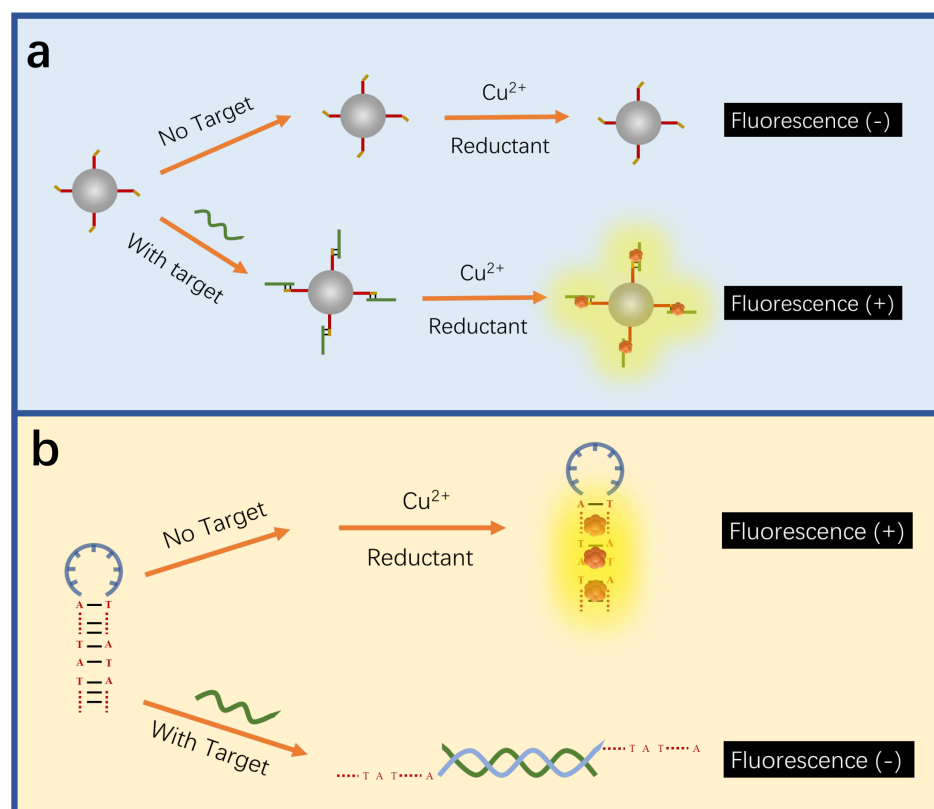
Figure 6. Schematic illustration of CuNC-based sensors. (**a**) The fluorescent detection based on the in situ formation of fluorescent CuNCs. The presence of a target produces favorable structures for generating fluorescent CuNCs, increasing the fluorescent intensity. Redrawn from [132]. (**b**) The fluorescent detection based on the non-formation of fluorescent CuNCs. The target destroys the hairpin structure, which favors the formation of fluorescent CuNCs, decreasing the fluorescent intensity. Redrawn from [134].

The hairpin structures of the adenine and thymine-rich DNA are more efficient in producing highly fluorescent CuNCs than other DNA structures [175] (Figure 6b). Moreover, this feature can also be utilized to probe DNA. Normally, the DNA hybridization between probes and analytes disrupts the hairpin structure, which is rich in adenine and thymine bases, causing a decrease in fluorescence intensity due to the disruption of CuNCs formation. For instance, Liu and others built up a qualitative and quantitative sensor for *chlamydia trachomatis* OMP1 gene, in which the target DNA can disrupt the hairpin structure of the probe for generating fluorescent CuNCs, leading to a decrease in fluorescence intensity [134]. The concentration of the target DNA is linearly correlated with the fluorescence intensity, and the detection limit is 18.5 nM. Liu and others reported a fluorescent sensor for the breast cancer 1 (BRCA1) gene, with a detection limit of 2 nM, and a good

recovery rate in bovine serum [135]. The target DNA hybridizes with the ring region of the hairpin probe, reducing the fluorescence intensity as a result of less formation of highly fluorescent CuNCs within the hairpin structure. The fluorescence intensity decreases with the increasing concentration of the BRCA1 gene.
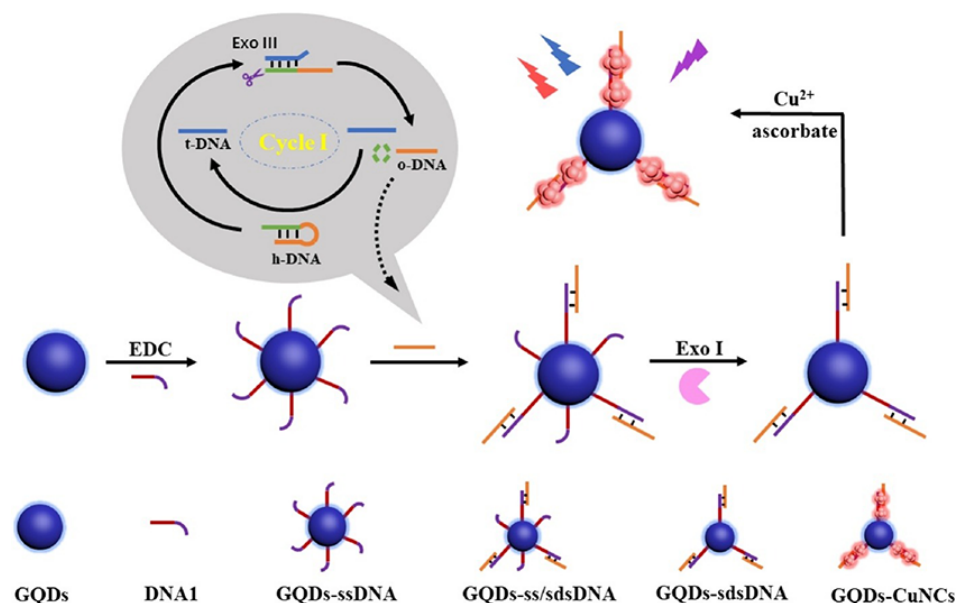

Figure 7. Schematic illustration of ratio fluorescence detection of HTLV-1 DNA based on the in situ generation of CuNCs on the DNA modified GQDs. Reproduced with permission from [132]. Copyright 2021 Elsevier.

A lower formation of CuNCs within DNA structures leads to a lower fluorescent intensity, which can be either caused by fewer as-formed highly fluorescent CuNCs, as indicated in the above-mentioned work, or more fluorescence quenchers, such as Cu^{2+} ions. Singh and others constructed a fluorescent sensor for DNA damage, utilizing Cu^{2+} ions [176], which are produced by the inhibition of CuNC formation, as the fluorescence quencher. Basic sites are present in the damaged part of DNA, hindering the generation of CuNCs within the structure and increasing the amount of Cu^{2+} ions in the solution. Cu^{2+} ions are then detected by fluorescent carbon dots, whose fluorescent intensity is proportionally quenched, quantitatively reflecting the presence of DNA damage.

In summary, adenine- and thymine-rich sequences and their hairpin structures favor the formation of fluorescent CuNCs, which can be utilized for CuNC-based sensors to detect DNA. Notably, the detection limit of CuNC-based DNA sensors can be as low as 0.54 pM, which is higher than those of their AgNC and AuNC counterparts. Compared with AuNCs and AgNCs, there are fewer reports on CuNC-based sensors for DNA detection, due to the intrinsically high difficulty in obtaining ultra-small CuNCs.

3.4. Alloy MNCs for DNA Detection

Alloy MNCs can show superior electronic and optical properties because of their multi-metal composition [177]. For example, bimetallic Au/AgNCs have a higher fluorescence quantum yield and better stability compared to AuNCs or AgNCs [178]. Multi-recognition molecular linking and the integration of multiple signals can optimize alloy nanoclusters (such as AuIAgNCS) for double or multi-target DNA detection. Bimetallic Cu/AuNCs also show enhanced fluorescence and a long fluorescent lifetime of 6.55 μs compared to AuNCs [179]. The enhanced performance makes alloy MNCs promising, sensitive and stable sensors for DNA detection.

Dehghani and others developed a rapid sensor for jejunum-bending bacteria DNA based on Au/AgNCs [136]. DNA detection is realized by hybridizing the DNA probe with the target DNA, which results in the fluorescence quenching of Au/AgNCs. The linear detection range is 10 to 30 pM, with a detection limit of 4.4 pM.

Compared with AgNCs, Ag/PtNCs show better homogeneity and peroxisase-like activity. Wu and others used DNA-templated Ag/PtNCs as an electrochemical probe, integrating it with a locked nucleic acid-modified X-shape probe for the identification of single nucleotide polymorphisms (Figure 8) [137]. The presence of target DNA triggers the strand displacement reaction between the target DNA and the X-type probe, leading to the division of the X-type probe to form Complex 1 and Complex 2. Complex 2, which remains bound to the electrode surface, can hybridize with the highly catalytic triplex-Ag/PtNCs to further catalyze the oxidation of methylene blue, leading to a substantial increase in electrical signals. The target concentration is proportional to the current, and the sensor has a detection limit of 0.8 fM.
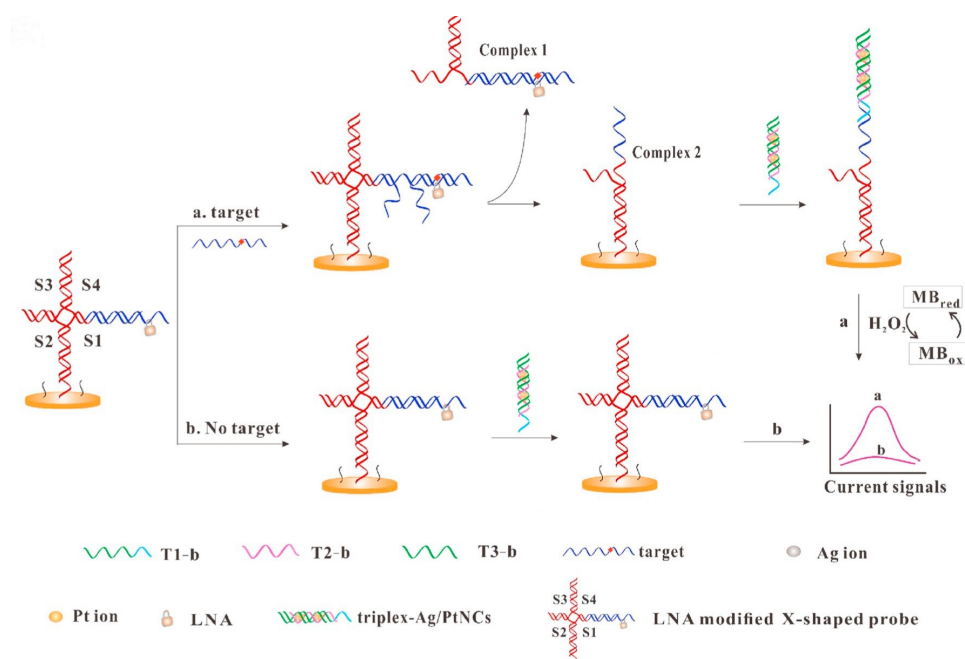
Figure 8. Schematic illustration of electrochemical detection of DNA based on the triplex-Ag/PtNCs and LNA-modified X-shaped DNA probe. Reproduced with permission from [137]. Copyright 2020 Elsevier.

The immediate detection of biomolecules is critical in cancer diagnosis [180], in which alloy NCs can serve as an effective sensor with high sensitivity. Wasfi et al. developed a graphite oxide-based field-effect transistor (FET) for real-time DNA detection, whose graphite oxide channel is modified by trimetal nanoclusters consisting of gold, silver and platinum, achieving a detection limit of 1.28 nM [138]. The presence of target DNA produces more holes in the channel to trap electrons, thereby increasing resistance and reducing current. The sensor's current decreases with the rising concentration of target DNA.

4. Conclusions

MNCs have attracted significant attention in biosensors due to their high photoluminescence performance, redox capabilities, and unique electronic structures. Currently, there are many synthetic methods to obtain MNCs. Various DNA amplification strategies, including the hybridization chain reaction strategy, the catalytic chain moving amplification and the target cycle amplification, have significantly enhanced the sensitivity of sensors.

Notably, the new CRISPR/Cas system is particularly useful in increasing detection limits. In recent decades, there has been rapid development in the biomedical detection of DNA with optical and electrochemical sensors based on MNCs. These sensors enable the early detection of DNA-related diseases, such as cancers and tumor metastasis, although some of them can be only used under certain clinical conditions. The stability of MNC-based sensors still needs improvement, which presents a great challenge. The stability of MNCs can be improved by selecting appropriate ligands and applying proper doping methods. The use of appropriate encapsulation materials for packaging biosensors and application of protective coatings can improve the stability and biocompatibility of MNC-based biosensors during long-term applications. However, alloy MNCs remain under-studied. Based on MNCs, sensors will play an increasingly important role in DNA detection. Moreover, there is a need to reduce interference factors in complex samples, overcoming the challenges of sensor integration and miniaturization. This is of great significance for the development and application of MNC-based sensors in the early detection of clinical diseases. Overall, biosensors based on MNCs have diverse detection capabilities. Besides being able to conduct precise detection in the early stage of DNA infection, they can also effectively monitor viral RNA. At the same time, they are capable of carrying out highly sensitive detection of cancer-related miRNA and epigenetic modifications, providing more comprehensive and in-depth technical support for the diagnosis and research in the biomedical field.

Author Contributions: Conceptualization, R.H.; validation, R.H. and S.W.; resources, R.H., S.W. and F.J.; data curation, R.H., S.W. and F.J.; writing—original draft preparation, R.H.; writing—review and editing, R.H., N.H. and L.N.; visualization R.H., N.H. and L.N.; supervision L.N., Z.H., Y.G. and J.Z. All authors have read and agreed to the published version of the manuscript.

Institutional Review Board Statement: Not applicable.

Informed Consent Statement: Not applicable.

Data Availability Statement: Not applicable.

Conflicts of Interest: The authors declare no conflicts of interest.

References

1. Jiang, P.; Wang, Y.; Zhao, L.; Ji, C.; Chen, D.; Nie, L. Applications of gold nanoparticles in non-optical biosensors. *Nanomaterials* **2018**, *8*, 977. [CrossRef] [PubMed]
2. Su, Y.; Xue, T.; Liu, Y.; Qi, J.; Jin, R.; Lin, Z. Luminescent metal nanoclusters for biomedical applications. *Nano Res.* **2019**, *12*, 1251–1265. [CrossRef]
3. Zheng, J.; Nicovich, P.R.; Dickson, R.M. Highly fluorescent noble-metal quantum dots. *Annu. Rev. Phys. Chem.* **2007**, *58*, 409–431. [CrossRef]
4. Shellaiah, M.; Sun, K.W. Luminescent metal nanoclusters for potential chemosensor applications. *Chemosensors* **2017**, *5*, 36. [CrossRef]
5. Chen, Y.; Phipps, M.L.; Werner, J.H.; Chakraborty, S.; Martinez, J.S. DNA templated metal nanoclusters: From emergent properties to unique applications. *Accounts Chem. Res.* **2018**, *51*, 2756–2763. [CrossRef] [PubMed]
6. Tao, Y.; Li, M.; Ren, J.; Qu, X. Metal nanoclusters: Novel probes for diagnostic and therapeutic applications. *Chem. Soc. Rev.* **2015**, *44*, 8636–8663. [CrossRef] [PubMed]
7. Li, R.D.; Wang, Q.; Yin, B.C.; Ye, B.C. Enzyme-free detection of sequence-specific microRNAs based on nanoparticle-assisted signal amplification strategy. *Biosens. Bioelectron.* **2016**, *77*, 995–1000. [CrossRef] [PubMed]
8. Yan, X.; Xie, H.; Wu, G.; Xiao, F.X. Boosted solar water oxidation steered by atomically precise alloy nanocluster. *Chin. Chem. Lett.* **2025**, *36*, 110279. [CrossRef]
9. Yang, J.; Peng, Y.; Li, S.; Mu, J.; Huang, Z.; Ma, J.; Shi, Z.; Jia, Q. Metal nanocluster-based hybrid Nanomaterials: Fabrication and application. *Coordin. Chem. Rev.* **2022**, *456*, 214391. [CrossRef]

10. Kwak, K.; Lee, D. Electrochemistry of atomically precise metal nanoclusters. *Accounts Chem. Res.* **2018**, *52*, 12–22. [CrossRef] [PubMed]

11. Zheng, K.; Xie, J. Engineering ultrasmall metal nanoclusters as promising theranostic agents. *Trends Chem.* **2020**, *2*, 665–679. [CrossRef]

12. Zhou, Y.; Mao, Z.; Xu, J.J. Recent advances in near infrared (NIR) electrochemiluminescence luminophores. *Chin. Chem. Lett.* **2024**, *35*, 109622. [CrossRef]

13. Li, D.; Wang, G.; Mei, X. Diagnosis of cancer at early stages based on the multiplex detection of tumor markers using metal nanoclusters. *Analyst* **2020**, *145*, 7150–7161. [CrossRef] [PubMed]

14. Srinivasulu, Y.G.; Mozhi, A.; Goswami, N.; Yao, Q.; Xie, J. Gold nanocluster based nanocomposites for combinatorial antibacterial therapy for eradicating biofilm forming pathogens. *Mater. Chem. Front.* **2022**, *6*, 689–706. [CrossRef]

15. Xiao, Y.; Wu, Z.; Yao, Q.; Xie, J. Luminescent metal nanoclusters: Biosensing strategies and bioimaging applications. *Aggregate* **2021**, *2*, 114–132. [CrossRef]

16. Vikrant, K.; Bhardwaj, N.; Bhardwaj, S.K.; Kim, K.H.; Deep, A. Nanomaterials as efficient platforms for sensing DNA. *Biomaterials* **2019**, *214*, 119215. [CrossRef] [PubMed]

17. Qi, H.; Xu, Y.; Hu, P.; Yao, C.; Yang, D. Construction and applications of DNA-based Nanomaterials in cancer therapy. *Chin. Chem. Lett.* **2022**, *33*, 1131–1140. [CrossRef]

18. Liu, J.; Zhang, L.; Zeng, W.; Zhang, L.; He, N.; Lu, Z. High-throughput quantitative detection of triple-negative breast cancer-associated expressed miRNAs by rolling circle amplification on fluorescence-encoded microspheres. *Chin. Chem. Lett.* **2023**, *34*, 108141. [CrossRef]

19. Zhou, X.; Pathak, P.; Jayawickramarajah, J. Design, synthesis, and applications of DNA–macrocyclic host conjugates. *Chem. Commun.* **2018**, *54*, 11668–11680. [CrossRef] [PubMed]

20. Guo, J.; Feng, C.; Liu, Z.; Ye, B.; Li, G.; Zou, L. A label-free electrochemical biosensor based on novel DNA nanotweezer coupled with G-quadruplex for sensitive DNA detection. *Sens. Actuators B Chem.* **2021**, *331*, 129437. [CrossRef]

21. Wang, H.F.; Ma, R.N.; Sun, F.; Jia, L.P.; Zhang, W.; Shang, L.; Xue, Q.W.; Jia, W.L.; Wang, H.S. A versatile label-free electrochemical biosensor for circulating tumor DNA based on dual enzyme assisted multiple amplification strategy. *Biosens. Bioelectron.* **2018**, *122*, 224–230. [CrossRef]

22. Cohen, P.A.; Jhingran, A.; Oaknin, A.; Denny, L. Cervical cancer. *Lancet* **2019**, *393*, 169–182. [CrossRef] [PubMed]

23. Hou, M.; Ma, L.; Yang, H.; Si, F.; Liu, Y. Background-free and signal-amplified upconversion fluorescent biosensing platform for sensitive detection of CYFRA21-1. *Talanta* **2023**, *262*, 124659. [CrossRef] [PubMed]

24. Kuang, H.; Zhao, S.; Chen, W.; Ma, W.; Yong, Q.; Xu, L.; Wang, L.; Xu, C. Rapid DNA detection by interface PCR on nanoparticles. *Biosens. Bioelectron.* **2011**, *26*, 2495–2499. [CrossRef]

25. Fang, Y.; Wang, Y.; Zhu, L.; Liu, H.; Su, X.; Liu, Y.; Chen, Z.; Chen, H.; He, N. A novel cartridge for nucleic acid extraction, amplification and detection of infectious disease pathogens with the help of magnetic nanoparticles. *Chin. Chem. Lett.* **2023**, *34*, 108092. [CrossRef]

26. Kirnbauer, R.; Hubbert, N.L.; Wheeler, C.M.; Becker, T.M.; Lowy, D.R.; Schiller, J.T. A virus-like particle enzyme-linked immunosorbent assay detects serum antibodies in a majority of women infected with human papillomavirus type 16. *JNCI J. Natl. Cancer Inst.* **1994**, *86*, 494–499. [CrossRef] [PubMed]

27. Shani, H.; Goldwaser, T.; Keating, J.; Klugman, S. Chromosomal abnormalities not currently detected by cell-free fetal DNA: A retrospective analysis at a single center. *Am. J. Obstet. Gynecol.* **2016**, *214*, 729.e1–729.e11. [CrossRef]

28. Wu, K.; Kong, F.; Zhang, J.; Tang, Y.; Chen, Y.; Chao, L.; Nie, L.; Huang, Z. Recent progress in single-nucleotide polymorphism biosensors. *Biosensors* **2023**, *13*, 864. [CrossRef]

29. Shi, N.; Jia, H.; Zhang, J.; Lu, P.; Cai, C.; Zhang, Y.; Zhang, L.; He, N.; Zhu, W.; Cai, Y.; et al. Accurate expression of neck motion signal by piezoelectric sensor data analysis. *Chin. Chem. Lett.* **2024**, *35*, 109302. [CrossRef]

30. Han, S.; Zhao, Y.; Zhang, Z.; Xu, G. Recent advances in electrochemiluminescence and chemiluminescence of metal nanoclusters. *Molecules* **2020**, *25*, 5208. [CrossRef] [PubMed]

31. Xie, J.L.; Xie, T.J.; Luo, Y.J.; Mao, K.; Huang, C.Z.; Li, Y.F.; Zhen, S.J. Octopus-like DNA nanostructure coupled with graphene oxide enhanced fluorescence anisotropy for hepatitis B virus DNA detection. *Chin. Chem. Lett.* **2024**, *35*, 109137. [CrossRef]

32. Xu, L.J.; Lei, Z.C.; Li, J.; Zong, C.; Yang, C.J.; Ren, B. Label-free surface-enhanced Raman spectroscopy detection of DNA with single-base sensitivity. *J. Am. Chem. Soc.* **2015**, *137*, 5149–5154. [CrossRef] [PubMed]

33. Loo, A.H.; Sofer, Z.; Bouša, D.; Ulbrich, P.; Bonanni, A.; Pumera, M. Carboxylic carbon quantum dots as a fluorescent sensing platform for DNA detection. *ACS Appl. Mater. Interfaces* **2016**, *8*, 1951–1957. [CrossRef]

34. Chen, W.; Fang, X.; Li, H.; Cao, H.; Kong, J. DNA-mediated inhibition of peroxidase-like activities on platinum nanoparticles for simple and rapid colorimetric detection of nucleic acids. *Biosens. Bioelectron.* **2017**, *94*, 169–175. [CrossRef] [PubMed]

35. Qian, S.; Wang, Z.; Zuo, Z.; Wang, X.; Wang, Q.; Yuan, X. Engineering luminescent metal nanoclusters for sensing applications. *Coordin. Chem. Rev.* **2022**, *451*, 214268. [CrossRef]

36. Yuan, X.; Luo, Z.; Yu, Y.; Yao, Q.; Xie, J. Luminescent noble metal nanoclusters as an emerging optical probe for sensor development. *Chem.-Asian J.* **2013**, *8*, 858–871. [CrossRef] [PubMed]

37. Chen, L.; Tang, Q.; Wu, S.; Zhang, L.; Feng, L.; Wang, Y.; Xie, Y.; Li, Y.; Zou, J.P.; Luo, S.L. Covalent coupling promoting charge transport of CdSeTe/UiO-66 for boosting photocatalytic CO_2 reduction. *Chin. Chem. Lett.* **2023**, *34*, 107903. [CrossRef]

38. Granger, J.H.; Schlotter, N.E.; Crawford, A.C.; Porter, M.D. Prospects for point-of-care pathogen diagnostics using surface-enhanced Raman scattering (SERS). *Chem. Soc. Rev.* **2016**, *45*, 3865–3882. [CrossRef] [PubMed]

39. Liu, B.; Yao, H.; Song, W.; Jin, L.; Mosa, I.M.; Rusling, J.F.; Suib, S.L.; He, J. Ligand-free noble metal nanocluster catalysts on carbon supports via "soft" nitriding. *J. Am. Chem. Soc.* **2016**, *138*, 4718–4721. [CrossRef]

40. Xue, R.; Geng, X.; Liang, F.; Liu, Y.; Yang, W.; Huang, Z. Natural plant compounds in synthesis and Luminescence modulation of metal nanoclusters: Toward sustainable nanoprobes for sensing and bioimaging. *Mater. Today Adv.* **2022**, *16*, 100279. [CrossRef]

41. Lu, Y.; Wei, W.; Chen, W. Copper nanoclusters: Synthesis, characterization and properties. *Chin. Sci. Bull.* **2012**, *57*, 41–47. [CrossRef]

42. Baghdasaryan, A.; Bürgi, T. Copper nanoclusters: Designed synthesis, structural diversity, and multiplatform applications. *Nanoscale* **2021**, *13*, 6283–6340. [CrossRef] [PubMed]

43. Yao, Q.; Chen, T.; Yuan, X.; Xie, J. Toward total synthesis of thiolate-protected metal nanoclusters. *Acc. Chem. Res.* **2018**, *51*, 1338–1348. [CrossRef]

44. Karpushkin, E.; Ivanova, N.; Lopatina, L.; Sergeyev, V. Fluorescent gold nanoclusters prepared in the presence of DNA. *Funct. Mater. Lett.* **2020**, *13*, 2041002. [CrossRef]

45. Zeng, C.; Chen, Y.; Li, G.; Jin, R. Magic size $Au_{64}(S-c-C_6H_{11})_{32}$ nanocluster protected by cyclohexanethiolate. *Chem. Mater.* **2014**, *26*, 2635–2641. [CrossRef]

46. Chen, W.; Chen, Y.; Zhu, X.; Xu, M.; Han, Z.; Wang, L.; Weng, L. $NaBH_4$-mediated co-reduction synthesis of glutathione stabilized gold/silver nanoclusters for detection of magnesium Ions. *Chemosensors* **2023**, *11*, 435. [CrossRef]

47. Nasirian, V.; Shamsipur, M.; Molaabasi, F.; Mansouri, K.; Sarparast, M.; Salim, V.; Barati, A.; Kashanian, S. miRNA-21 rapid diagnosis by one-pot synthesis of highly luminescent red emissive silver nanoclusters/DNA. *Sens. Actuators B Chem.* **2020**, *308*, 127673. [CrossRef]

48. Wang, Y.; Chen, T.; Zhuang, Q.; Ni, Y. One-pot aqueous synthesis of nucleoside-templated fluorescent copper nanoclusters and their application for discrimination of nucleosides. *ACS Appl. Mater. Interfaces* **2017**, *9*, 32135–32141. [CrossRef]

49. Tiwari, N.; Mishra, R.K.; Gupta, S.; Srivastava, R.; Aggarwal, S.; Bandyopadhyay, P.; Munde, M. Synthetic tunability and biophysical basis for fabricating highly fluorescent and stable DNA copper nanoclusters. *Langmuir* **2021**, *37*, 9385–9395. [CrossRef]

50. Katla, S.K.; Zhang, J.; Castro, E.; Bernal, R.A.; Li, X. Atomically precise $Au_{25}(SG)_{18}$ nanoclusters: Rapid single-step synthesis and application in photothermal therapy. *ACS Appl. Mater. Interfaces* **2018**, *10*, 75–82. [CrossRef] [PubMed]

51. Yan, W.; Zhang, J.; Abbas, M.; Li, Y.; Hussain, S.Z.; Mumtaz, S.; Song, Z.; Hussain, I.; Tan, B. Facile synthesis of ultrastable fluorescent copper nanoclusters and their cellular imaging application. *Nanomaterials* **2020**, *10*, 1678. [CrossRef] [PubMed]

52. Zeng, C.; Chen, Y.; Das, A.; Jin, R. Transformation chemistry of gold nanoclusters: From one stable size to another. *J. Phys. Chem. Lett.* **2015**, *6*, 2976–2986. [CrossRef] [PubMed]

53. Liu, C.; Lin, J.; Shi, Y.; Li, G. Efficient synthesis of $Au_{99}(SR)_{42}$ nanoclusters. *Nanoscale* **2015**, *7*, 5987–5990. [CrossRef] [PubMed]

54. Liu, C.; Yan, C.; Lin, J.; Yu, C.; Huang, J.; Li, G. One-pot synthesis of $Au_{144}(SCH_2Ph)_{60}$ nanoclusters and their catalytic application. *J. Mater. Chem. A* **2015**, *3*, 20167–20173. [CrossRef]

55. Shichibu, Y.; Negishi, Y.; Tsukuda, T.; Teranishi, T. Large-scale synthesis of thiolated Au_{25} clusters via ligand exchange reactions of phosphine-stabilized Au11 clusters. *J. Am. Chem. Soc.* **2005**, *127*, 13464–13465. [CrossRef]

56. Shah, P.; Rørvig-Lund, A.; Chaabane, S.B.; Thulstrup, P.W.; Kjaergaard, H.G.; Fron, E.; Hofkens, J.; Yang, S.W.; Vosch, T. Design aspects of bright red emissive silver nanoclusters/DNA probes for microRNA detection. *ACS Nano* **2012**, *6*, 8803–8814. [CrossRef]

57. Ganguly, M.; Pal, A.; Negishi, Y.; Pal, T. Synthesis of highly fluorescent silver clusters on gold (I) surface. *Langmuir* **2013**, *29*, 2033–2043. [CrossRef]

58. Qu, F.; Li, N.B.; Luo, H.Q. Highly sensitive fluorescent and colorimetric pH sensor based on polyethylenimine-capped silver nanoclusters. *Langmuir* **2013**, *29*, 1199–1205. [CrossRef]

59. Gregersen, S.; Vosch, T.; Jensen, K.J. Peptide-stabilized, fluorescent silver nanoclusters: Solid-hhase synthesis and screening. *Chem.-Asian J.* **2016**, *22*, 18492–18500. [CrossRef] [PubMed]

60. Yu, Y.; Geng, J.; Ong, E.Y.X.; Chellappan, V.; Tan, Y.N. Bovine serum albumin protein-templated silver nanocluster ($BSA-Ag_{13}$): An effective singlet oxygen generator for photodynamic cancer therapy. *Adv. Healthc. Mater.* **2016**, *5*, 2528–2535. [CrossRef] [PubMed]

61. Chang, W.T.; Lee, P.Y.; Liao, J.H.; Chakrahari, K.K.; Kahlal, S.; Liu, Y.C.; Chiang, M.H.; Saillard, J.Y.; Liu, C. Eight-electron silver and mixed gold/silver nanoclusters stabilized by selenium donor ligands. *Angew. Chem. Int. Ed.* **2017**, *56*, 10178–10182. [CrossRef]

62. Bootharaju, M.S.; Joshi, C.P.; Alhilaly, M.J.; Bakr, O.M. Switching a nanocluster core from hollow to nonhollow. *Chem. Mater.* **2016**, *28*, 3292–3297. [CrossRef]

63. Nguyen, T.A.D.; Jones, Z.R.; Leto, D.F.; Wu, G.; Scott, S.L.; Hayton, T.W. Ligand-exchange-induced growth of an atomically precise Cu_{29} nanocluster from a smaller cluster. *Chem. Mater.* **2016**, *28*, 8385–8390. [CrossRef]

64. Cui, H.; Shao, Z.S.; Song, Z.; Wang, Y.B.; Wang, H.S. Development of gold nanoclusters: From preparation to applications in the field of biomedicine. *J. Mater. Chem. C* **2020**, *8*, 14312–14333. [CrossRef]

65. Wang, Z.; Chen, B.; Rogach, A.L. Synthesis, optical properties and applications of light-emitting copper nanoclusters. *Nanoscale Horiz.* **2017**, *2*, 135–146. [CrossRef]

66. Le Guével, X.; Spies, C.; Daum, N.; Jung, G.; Schneider, M. Highly fluorescent silver nanoclusters stabilized by glutathione: A promising fluorescent label for bioimaging. *Nano Res.* **2012**, *5*, 379–387. [CrossRef]

67. Chen, Y.; Dong, X.; Zheng, Y.; Wang, Y.; Guo, Z.; Jiang, H.; Wang, X. A novel turn-on fluorescent sensor for the sensitive detection of glutathione via gold nanocluster preparation based on controllable ligand-induced etching. *Analyst* **2020**, *145*, 4265–4275. [CrossRef]

68. Liu, C.; Ding, Y.; Li, Q.; Lin, Y. Photochemical synthesis of glutathione-stabilized silver nanoclusters for fluorometric determination of hydrogen peroxide. *Microchim. Acta* **2017**, *184*, 2497–2503. [CrossRef]

69. Shen, Q.; Hossain, F.; Fang, C.; Shu, T.; Zhang, X.; Law, J.L.M.; Logan, M.; Houghton, M.; Tyrrell, D.L.; Joyce, M.A.; et al. Bovine serum albumin-protected gold nanoclusters for sensing of SARS-CoV-2 antibodies and virus. *ACS Appl. Mater. Interfaces* **2023**, *15*, 29914–29926. [CrossRef]

70. Deng, H.H.; Li, K.L.; Zhuang, Q.Q.; Peng, H.P.; Zhuang, Q.Q.; Liu, A.L.; Xia, X.H.; Chen, W. An ammonia-based etchant for attaining copper nanoclusters with green fluorescence emission. *Nanoscale* **2018**, *10*, 6467–6473. [CrossRef]

71. Saleh, S.M.; El-Sayed, W.A.; El-Manawaty, M.A.; Gassoumi, M.; Ali, R. An eco-friendly synthetic approach for copper nanoclusters and their potential in lead ions sensing and biological applications. *Biosensors* **2022**, *12*, 197. [CrossRef] [PubMed]

72. Sadhu, V.A.; Jha, S.; Park, T.J.; Kailasa, S.K. Synthesis of copper nanoclusters from Bacopa monnieri leaves for fluorescence sensing of dichlorvos. *Luminescence* **2023**, *38*, 1872–1882. [CrossRef] [PubMed]

73. Li, R.; Wang, C.; Bo, F.; Wang, Z.; Shao, H.; Xu, S.; Cui, Y. Microwave-assisted synthesis of fluorescent Ag nanoclusters in aqueous solution. *ChemPhysChem* **2012**, *13*, 2097–2101. [CrossRef] [PubMed]

74. Naaz, S.; Chowdhury, P. Sunlight and ultrasound-assisted synthesis of photoluminescent silver nanoclusters: A unique 'knock out' sensor for thiophilic metal ions. *Sens. Actuators B Chem.* **2017**, *241*, 840–848. [CrossRef]

75. Zhang, G.; Xu, T.; Du, H.; Qiao, Y.; Guo, X.; Shi, L.; Zhang, Y.; Shuang, S.; Dong, C.; Ma, H. A reversible fluorescent pH-sensing system based on the one-pot synthesis of natural silk fibroin-capped copper nanoclusters. *J. Mater. Chem. C* **2016**, *4*, 3540–3545. [CrossRef]

76. Xu, F.; Qing, T.; Qing, Z. DNA-coded metal nano-fluorophores: Preparation, properties and applications in biosensing and bioimaging. *Nano Today* **2021**, *36*, 101021. [CrossRef]

77. Ning, L.; Li, Y.; Zhang, Z.; Zhou, Y.; Yang, L.; Yu, Q.; Yu, F.; Tong, Z. Primer exchange reaction coupled with DNA-templated silver nanoclusters for label-free and sensitive detection of microRNA. *Appl. Biochem. Biotech.* **2023**, *195*, 6334–6344. [CrossRef] [PubMed]

78. Zhang, Y.; Liao, Y.; Yin, X.; Zhang, Y.; Yang, Z.; Wang, H.; Yang, W.; Pang, P. Electrochemical determination of Pb^{2+} based on DNAzyme-triggered rolling circle amplification and DNA-templated silver nanoclusters amplification strategy. *Microchem. J.* **2023**, *189*, 108544. [CrossRef]

79. Huang, R.; He, L.; Jin, L.; Li, Z.; He, N.; Miao, W. Recent advancements in DNA nanotechnology-enabled extracellular vesicles detection and diagnosis: A mini review. *Chin. Chem. Lett.* **2023**, *34*, 107926. [CrossRef]

80. Tan, S.C.L.; He, Z.; Wang, G.; Yu, Y.; Yang, L. Protein-templated metal nanoclusters: Molecular-like hybrids for biosensing, diagnostics and pharmaceutics. *Molecules* **2023**, *28*, 5531. [CrossRef]

81. Aires, A.; Lopez-Martinez, E.; Cortajarena, A.L. Sensors based on metal nanoclusters stabilized on designed proteins. *Biosensors* **2018**, *8*, 110. [CrossRef]

82. Yang, C.; Shi, K.; Dou, B.; Xiang, Y.; Chai, Y.; Yuan, R. In situ DNA-templated synthesis of silver nanoclusters for ultrasensitive and label-free electrochemical detection of microRNA. *ACS Appl. Mater. Interfaces* **2015**, *7*, 1188–1193. [CrossRef] [PubMed]

83. Shen, C.; Xia, X.; Hu, S.; Yang, M.; Wang, J. Silver nanoclusters-based fluorescence assay of protein kinase activity and inhibition. *Anal. Chem.* **2015**, *87*, 693–698. [CrossRef] [PubMed]

84. Yuan, Z.; Chen, Y.C.; Li, H.W.; Chang, H.T. Fluorescent silver nanoclusters stabilized by DNA scaffolds. *Chem. Commun.* **2014**, *50*, 9800–9815. [CrossRef]

85. Thyrhaug, E.; Bogh, S.A.; Carro-Temboury, M.R.; Madsen, C.S.; Vosch, T.; Zigmantas, D. Ultrafast coherence transfer in DNA-templated silver nanoclusters. *Nat. Commun.* **2017**, *8*, 15577. [CrossRef]

86. Obliosca, J.M.; Liu, C.; Yeh, H.C. Fluorescent silver nanoclusters as DNA probes. *Nanoscale* **2013**, *5*, 8443–8461. [CrossRef]

87.　Yao, Y.; Li, N.; Zhang, X.; Ong'achwa Machuki, J.; Yang, D.; Yu, Y.; Li, J.; Tang, D.; Tian, J.; Gao, F. DNA-templated silver nanocluster/porphyrin/MnO$_2$ platform for label-free intracellular Zn^{2+} imaging and fluorescence-/magnetic resonance imaging-guided photodynamic therapy. *ACS Appl. Mater. Interfaces* **2019**, *11*, 13991–14003. [CrossRef] [PubMed]

88.　Lv, Z.; Huang, M.; Li, P.; Xu, M.; Yao, C.; Yang, D. Hybridization chain reaction-based DNA Nanomaterials for biosensing, bioimaging and therapeutics. *Chin. Chem. Lett.* **2024**, *35*, 108601. [CrossRef]

89.　Lee, S.Y.; Bahara, N.H.H.; Choong, Y.S.; Lim, T.S.; Tye, G.J. DNA fluorescence shift sensor: A rapid method for the detection of DNA hybridization using silver nanoclusters. *J. Colloid Interface Sci.* **2014**, *433*, 183–188. [CrossRef] [PubMed]

90.　Zhou, W.; Zhu, J.; Fan, D.; Teng, Y.; Zhu, X.; Dong, S. A multicolor chameleon DNA-templated silver nanocluster and Its application for ratiometric fluorescence target detection with exponential signal response. *Adv. Funct. Mater.* **2017**, *27*, 1704092. [CrossRef]

91.　Ye, Y.D.; Xia, L.; Xu, D.D.; Xing, X.J.; Pang, D.W.; Tang, H.W. DNA-stabilized silver nanoclusters and carbon nanoparticles oxide: A sensitive platform for label-free fluorescence turn-on detection of HIV-DNA sequences. *Biosens. Bioelectron.* **2016**, *85*, 837–843. [CrossRef] [PubMed]

92.　Zhang, Y.; Mu, F.; Duan, Y.; Li, Q.; Pan, Y.; Du, H.; He, P.; Shen, X.; Luo, Z.; Zhu, C.; et al. Label-free analysis of H5N1 virus based on three-segment branched DNA-templated fluorescent silver nanoclusters. *ACS Appl. Mater. Interfaces* **2020**, *12*, 48357–48362. [CrossRef] [PubMed]

93.　Shen, F.; Qian, H.; Cheng, Y.; Xie, Y.; Yu, H.; Yao, W.; Pei, R.; Guo, Y.; Li, H.W. Three-way junction-promoted recycling amplification for sensitive DNA detection using highly bright DNA-silver nanocluster as label-free output. *Talanta* **2020**, *206*, 120216. [CrossRef] [PubMed]

94.　Li, W.; Liu, C.; Liu, D.; Liu, S.; You, T. Ratiometric fluorescent sensing of mercury (II) ion based on the Pt nanozyme-triggered fluorescence resonance energy transfer between Si quantum dots and 2,3-diaminophenazine. *Sens. Actuators B Chem.* **2021**, *331*, 112976. [CrossRef]

95.　Liu, L.; Ga, L.; Ai, J. Ratiometric fluorescence sensing with logical operation: Theory, design and applications. *Biosens. Bioelectron.* **2022**, *213*, 114456. [CrossRef]

96.　Liu, X.; Hu, R.; Gao, Z.; Shao, N. Photoluminescence mechanism of DNA-templated silver nanoclusters: Coupling between surface plasmon and emitter and sensing of lysozyme. *Langmuir* **2015**, *31*, 5859–5867. [CrossRef]

97.　Ritchie, C.M.; Johnsen, K.R.; Kiser, J.R.; Antoku, Y.; Dickson, R.M.; Petty, J.T. Ag nanocluster formation using a cytosine oligonucleotide template. *J. Phys. Chem. Lett.* **2007**, *111*, 175–181. [CrossRef]

98.　Sengupta, B.; Ritchie, C.M.; Buckman, J.G.; Johnsen, K.R.; Goodwin, P.M.; Petty, J.T. Base-directed formation of fluorescent silver clusters. *J. Phys. Chem. Lett.* **2008**, *112*, 18776–18782. [CrossRef]

99.　Wu, N.; Zhang, H.C.; Sun, X.H.; Guo, F.N.; Feng, L.X.; Yang, T.; Wang, J.H. Detection of HIV/HCV virus DNA with homogeneous DNA machine-triggered in situ formation of silver nanoclusters. *Sens. Actuators B Chem.* **2022**, *352*, 131041. [CrossRef]

100.　Zou, R.; Zhang, F.; Chen, C.; Cai, C. DNA-programming multicolor silver nanoclusters for sensitively simultaneous detection of two HIV DNAs. *Sens. Actuators B Chem.* **2019**, *296*, 126608. [CrossRef]

101.　Deféver, T.; Druet, M.; Evrard, D.; Marchal, D.; Limoges, B. Real-time electrochemical PCR with a DNA intercalating redox probe. *Anal. Chem.* **2011**, *83*, 1815–1821. [CrossRef] [PubMed]

102.　Chen, Y.; Xu, J.; Su, J.; Xiang, Y.; Yuan, R.; Chai, Y. In situ hybridization chain reaction amplification for universal and highly sensitive electrochemiluminescent detection of DNA. *Anal. Chem.* **2012**, *84*, 7750–7755. [CrossRef]

103.　Hu, Y.; Xu, X.; Liu, Q.; Wang, L.; Lin, Z.; Chen, G. Ultrasensitive electrochemical biosensor for detection of DNA from Bacillus subtilis by coupling target-induced strand displacement and nicking endonuclease signal amplification. *Anal. Chem.* **2014**, *86*, 8785–8790. [CrossRef]

104.　Zhang, J.; Hou, M.; Chen, G.; Mao, H.; Chen, W.; Wang, W.; Chen, J. An electrochemical biosensor based on DNA "nano-bridge" for amplified detection of exosomal microRNAs. *Chin. Chem. Lett.* **2021**, *32*, 3474–3478. [CrossRef]

105.　Ma, J.; Gong, L.; Cen, Y.; Feng, L.; Su, Y.; Liu, X.; Chao, J.; Wan, Y.; Su, S.; Wang, L. Electrochemical analysis of microRNAs with hybridization chain reaction-based triple signal amplification. *Chin. Chem. Lett.* **2023**, *34*, 108012. [CrossRef]

106.　Li, H.; Wang, X.; Wei, S.; Zhao, C.; Song, X.; Xu, K.; Li, J.; Pang, B.; Wang, J. Applications of hybridization chain reaction optical detection incorporating Nanomaterials: A review. *Anal. Chim. Acta* **2022**, *1190*, 338930. [CrossRef] [PubMed]

107.　Wu, J.; Lv, J.; Zheng, X.; Wu, Z.S. Hybridization chain reaction and its applications in biosensing. *Talanta* **2021**, *234*, 122637. [CrossRef] [PubMed]

108.　Wong, Z.W.; New, S.Y. An enzyme-free turn-on fluorescent strategy for nucleic acid detection based on hybridization chain reaction and transferable silver nanoclusters. *Microchim. Acta* **2023**, *190*, 16. [CrossRef]

109.　Chen, Z.; Liu, Y.; Xin, C.; Zhao, J.; Liu, S. A cascade autocatalytic strand displacement amplification and hybridization chain reaction event for label-free and ultrasensitive electrochemical nucleic acid biosensing. *Biosens. Bioelectron.* **2018**, *113*, 1–8. [CrossRef]

110. Liu, H.; You, Y.; Zhu, Y.; Zheng, H. Recent advances in the exonuclease III-assisted target signal amplification strategy for nucleic acid detection. *Anal. Methods* **2021**, *13*, 5103–5119. [CrossRef] [PubMed]

111. Zhang, K.; Yang, L.; Lu, F.; Wu, X.; Zhu, J.J. A universal upconversion sensing platform for the sensitive detection of tumour-related ncRNA through an Exo III-assisted cycling amplification strategy. *Small* **2018**, *14*, 1703858. [CrossRef] [PubMed]

112. Shi, H.; Jin, T.; Zhang, J.; Huang, X.; Tan, C.; Jiang, Y.; Tan, Y. A novel aptasensor strategy for protein detection based on G-quadruplex and exonuclease III-aided recycling amplification. *Chin. Chem. Lett.* **2020**, *31*, 155–158. [CrossRef]

113. Li, Z.M.; Zhong, Z.H.; Liang, R.P.; Qiu, J.D. The colorimetric assay of DNA methyltransferase activity based on strand displacement amplification. *Sens. Actuators B Chem.* **2017**, *238*, 626–632. [CrossRef]

114. Yang, X.; Liu, X.; Kang, Q.; Qi, Y.; Du, Y.; Xiang, H. A novel DNA detection using spherical identification probe and strand displacement reaction-initiated silver nanocluster switch. *Anal. Sci.* **2023**, *39*, 275–284. [CrossRef]

115. Qian, J.; Yang, Y.; Gong, F.; Shan, X.; Ji, X.; He, Z. Ratiometric fluorescence biosensing of silver NanoCluster Beacons for ATP detection based on ligation-triggered rolling cycle amplification. *Microchem. J.* **2023**, *190*, 108663. [CrossRef]

116. Kuo, Y.A.; Jung, C.; Chen, Y.A.; Kuo, H.C.; Zhao, O.S.; Nguyen, T.D.; Rybarski, J.R.; Hong, S.; Chen, Y.I.; Wylie, D.C.; et al. Massively parallel selection of nanocluster beacons. *Adv. Mater.* **2022**, *34*, 2204957. [CrossRef]

117. Feng, D.Q.; Zhang, W.; Wang, W.; Liu, G. Smart flared-nanokites with ultra-high fluorescence enhancement for multiplexing virus DNA biosensing. *Sens. Actuators B Chem.* **2023**, *387*, 133813. [CrossRef]

118. Ge, L.; Sun, X.; Hong, Q.; Li, F. Ratiometric catalyzed-assembly of nanocluster beacons: A nonenzymatic approach for amplified DNA detection. *ACS Appl. Mater. Interfaces* **2017**, *9*, 32089–32096. [CrossRef] [PubMed]

119. Ge, L.; Sun, X.; Hong, Q.; Li, F. Ratiometric NanoCluster Beacon: A label-free and sensitive fluorescent DNA detection platform. *ACS Appl. Mater. Interfaces* **2017**, *9*, 13102–13110. [CrossRef]

120. Liu, L.; Zhu, S.; Sun, J.; Xia, M.; Xu, G. Ratiometric fluorescence detection of bleomycin based on proximity-dependent fluorescence conversion of DNA-templated silver nanoclusters. *Chin. Chem. Lett.* **2021**, *32*, 906–909. [CrossRef]

121. Chen, Y.; Yin, D.; Ma, Y.; Bie, Z.; Liu, Z. Multimodal plasmonic assay of copper (II) ion via stimuli-responsive state transformation of silver molecular nanoparticles. *Anal. Chem.* **2016**, *88*, 8123–8128. [CrossRef]

122. Liu, G.; Li, J.; Feng, D.Q.; Zhu, J.J.; Wang, W. Silver nanoclusters beacon as stimuli-responsive versatile platform for multiplex DNAs detection and aptamer–substrate complexes sensing. *Anal. Chem.* **2017**, *89*, 1002–1008. [CrossRef] [PubMed]

123. Shamsipur, M.; Samandari, L.; Farzin, L.; Molaabasi, F.; Mousazadeh, M.H. Dual-modal label-free genosensor based on hemoglobin@ gold nanocluster stabilized graphene nanosheets for the electrochemical detection of BCR/ABL fusion gene. *Talanta* **2020**, *217*, 121093. [CrossRef] [PubMed]

124. Wang, W.; Bao, T.; Zeng, X.; Xiong, H.; Wen, W.; Zhang, X.; Wang, S. Ultrasensitive electrochemical DNA biosensor based on functionalized gold clusters/graphene nanohybrids coupling with exonuclease III-aided cascade target recycling. *Biosens. Bioelectron.* **2017**, *91*, 183–189. [CrossRef]

125. Wang, Y.; Bai, X.; Wen, W.; Zhang, X.; Wang, S. Ultrasensitive electrochemical biosensor for HIV gene detection based on graphene stabilized gold nanoclusters with exonuclease amplification. *ACS Appl. Mater. Interfaces* **2015**, *7*, 18872–18879. [CrossRef]

126. Tang, Z.; Chen, F.; Wang, D.; Xiong, D.; Yan, S.; Liu, S.; Tang, H. Fabrication of avidin-stabilized gold nanoclusters with dual emissions and their application in biosensing. *J. Nanobiotechnol.* **2022**, *20*, 306. [CrossRef]

127. Wang, H.B.; Bai, H.Y.; Dong, G.L.; Liu, Y.M. DNA-templated Au nanoclusters coupled with proximity-dependent hybridization and guanine-rich DNA induced quenching: A sensitive fluorescent biosensing platform for DNA detection. *Nanoscale Adv.* **2019**, *1*, 1482–1488. [CrossRef] [PubMed]

128. Hong, G.; Zou, Z.; Huang, Z.; Deng, H.; Chen, W.; Peng, H. Split-type electrochemiluminescent gene assay platform based on gold nanocluster probe for human papillomavirus diagnosis. *Biosens. Bioelectron.* **2021**, *178*, 113044. [CrossRef] [PubMed]

129. Liu, P.F.; Zhao, K.R.; Liu, Z.J.; Wang, L.; Ye, S.Y.; Liang, G.X. Cas12a-based electrochemiluminescence biosensor for target amplification-free DNA detection. *Biosens. Bioelectron.* **2021**, *176*, 112954. [CrossRef]

130. Guo, T.; Li, W.; Qian, L.; Yan, X.; Cui, D.; Zhao, J.; Ni, H.; Zhao, X.; Zhang, Z.; Li, X.; et al. Highly-selective detection of EGFR mutation gene in lung cancer based on surface enhanced Raman spectroscopy and asymmetric PCR. *J. Pharmaceut. Biomed.* **2020**, *190*, 113522. [CrossRef] [PubMed]

131. Chen, J.; Wang, M.; Bao, Y.; Xie, X.; Nie, Y.; Lv, Y.; Su, X. Construction of a sensing platform based on DNA-encoded magnetic beads and copper nanoclusters for viral gene analysis with target recycling amplification. *ACS Appl. Bio Mater.* **2021**, *4*, 5669–5677. [CrossRef] [PubMed]

132. Chen, J.; Wang, M.; Zhou, X.; Nie, Y.; Su, X. Highly sensitive label-free fluorescence determination of lymphotropic virus DNA based on exonuclease assisted target recycling amplification and in-situ generation of fluorescent copper nanoclusters. *Sens. Actuators B Chem.* **2021**, *326*, 128847. [CrossRef]

133. Tao, Y.; Yi, K.; Wang, H.; Li, K.; Li, M. Metal nanoclusters combined with CRISPR-Cas12a for hepatitis B virus DNA detection. *Sens. Actuators B Chem.* **2022**, *361*, 131711. [CrossRef]

134. Liu, L.; Bai, Q.; Zhang, X.; Lu, C.; Li, Z.; Liang, H.; Chen, L. Fluorescent biosensor based on hairpin DNA stabilized copper nanoclusters for chlamydia trachomatis detection. *J. Fluoresc.* **2022**, *32*, 1651–1660. [CrossRef] [PubMed]

135. Liu, J.; Wang, T.; Xiao, B.; Deng, M.; Yu, P.; Qing, T. Fluorometric determination of the breast cancer 1 gene based on the target-induced conformational change of a DNA template for copper nanoclusters. *Anal. Methods* **2021**, *13*, 712–718. [CrossRef] [PubMed]

136. Dehghani, Z.; Hosseini, M.; Mohammadnejad, J. A fluorescence nanobiosensor for detection of Campylobacter jejuni DNA in milk based on Au/Ag bimetallic nanoclusters. *J. Food Meas. Character.* **2019**, *13*, 1797–1804. [CrossRef]

137. Wu, F.; Lin, Q.; Wang, L.; Zou, Y.; Chen, M.; Xia, Y.; Lan, J.; Chen, J. A DNA electrochemical biosensor based on triplex DNA-templated Ag/Pt nanoclusters for the detection of single-nucleotide variant. *Talanta* **2020**, *207*, 120257. [CrossRef]

138. Wasfi, A.; Awwad, F.; Qamhieh, N.; Iratni, R.; Ayesh, A.I. Real-time nucleic acid detection via field-effect transistor sensors based on graphite oxide decorated with trimetallic nanocluster of gold, silver, and platinum. *New J. Phys.* **2021**, *23*, 103041. [CrossRef]

139. Zhang, Y.; Jiang, H.; Wang, X. Cytidine-stabilized gold nanocluster as a fluorescence turn-on and turn-off probe for dual functional detection of Ag^+ and Hg^{2+}. *Anal. Chim. Acta* **2015**, *870*, 1–7. [CrossRef] [PubMed]

140. Halawa, M.; Lai, J.; Xu, G. Gold nanoclusters: Synthetic strategies and recent advances in fluorescent sensing. *Mater. Today Nano* **2018**, *3*, 9–27. [CrossRef]

141. Xie, J.; Zheng, Y.; Ying, J.Y. Protein-directed synthesis of highly fluorescent gold nanoclusters. *J. Am. Chem. Soc.* **2009**, *131*, 888–889. [CrossRef] [PubMed]

142. Yao, Q.; Yuan, X.; Fung, V.; Yu, Y.; Leong, D.T.; Jiang, D.e.; Xie, J. Understanding seed-mediated growth of gold nanoclusters at molecular level. *Nat. Commun.* **2017**, *8*, 927. [CrossRef] [PubMed]

143. Li, L.; Liu, H.; Shen, Y.; Zhang, J.; Zhu, J.J. Electrogenerated chemiluminescence of Au nanoclusters for the detection of dopamine. *Anal. Chem.* **2011**, *83*, 661–665. [CrossRef] [PubMed]

144. Shamsipur, M.; Farzin, L.; Tabrizi, M.A.; Molaabasi, F. Highly sensitive label free electrochemical detection of VGEF165 tumor marker based on "signal off" and "signal on" strategies using an anti-VEGF165 aptamer immobilized BSA-gold nanoclusters/ionic liquid/glassy carbon electrode. *Biosens. Bioelectron.* **2015**, *74*, 369–375. [CrossRef]

145. Zhou, X.; Wang, X.; Shang, L. Ratiometric fluorescence and visual sensing of ATP based on gold nanocluster-encapsulated metal-organic framework with a smartphone. *Chin. Chem. Lett.* **2023**, *34*, 108093. [CrossRef]

146. Bao, Y.; Yeh, H.C.; Zhong, C.; Ivanov, S.A.; Sharma, J.K.; Neidig, M.L.; Vu, D.M.; Shreve, A.P.; Dyer, R.B.; Werner, J.H.; et al. Formation and stabilization of fluorescent gold nanoclusters using Small Molecules. *J. Phys. Chem. C* **2010**, *114*, 15879–15882. [CrossRef]

147. Zheng, J.; Petty, J.T.; Dickson, R.M. High quantum yield blue emission from water-soluble Au_8 nanodots. *J. Am. Chem. Soc.* **2003**, *125*, 7780–7781. [CrossRef]

148. Zhang, Z.; Liu, T.; Wang, S.; Ma, J.; Zhou, T.; Wang, F.; Wang, X.; Zhang, G. DNA-templated gold nanocluster as a novel fluorometric sensor for glutathione determination. *J. Photochem. Photobiol. A* **2019**, *370*, 89–93. [CrossRef]

149. Yang, X.; Shi, M.; Zhou, R.; Chen, X.; Chen, H. Blending of $HAuCl_4$ and histidine in aqueous solution: A simple approach to the Au_{10} cluster. *Nanoscale* **2011**, *3*, 2596–2601. [CrossRef] [PubMed]

150. Li, Y.; Cao, Y.; Wei, L.; Wang, J.; Zhang, M.; Yang, X.; Wang, W.; Yang, G. The assembly of protein-templated gold nanoclusters for enhanced fluorescence emission and multifunctional applications. *Acta Biomater.* **2020**, *101*, 436–443. [CrossRef]

151. Huang, Q.; Lin, X.; Tong, L.; Tong, Q.X. Graphene quantum dots/multiwalled carbon nanotubes composite-based electrochemical sensor for detecting dopamine release from living cells. *ACS Sustain. Chem. Eng.* **2020**, *8*, 1644–1650. [CrossRef]

152. Hosseini, S.M.; Imanpour, A.; Rezavand, M.; Arjmandi Tash, A.M.; Antonini, S.; Rezvani, S.J.; Abdi, Y. Electrochemoresistance sensor: A borophene-based sensor with simultaneous electrochemical and chemoresistance sensing capability. *ACS Mater. Lett.* **2024**, *6*, 933–942. [CrossRef]

153. Li, M.; Wang, X.; Zhu, Y.; Jia, X.; Zhang, S.; Wang, H.; Li, Y.; Hu, G. Fe_2O_3-decorated boron/nitrogen-co-doped carbon nanosheets as an electrochemical sensing platform for ultrasensitive determination of paraquat in natural water. *Chin. Chem. Lett.* **2023**, *34*, 107299. [CrossRef]

154. Liu, Y.; Jiang, D.; Wang, S.; Cai, G.; Xue, L.; Li, Y.; Liao, M.; Lin, J. A microfluidic biosensor for rapid detection of Salmonella typhimurium based on magnetic separation, enzymatic catalysis and electrochemical impedance analysis. *Chin. Chem. Lett.* **2022**, *33*, 3156–3160. [CrossRef]

155. Danis, A.S.; Potts, K.P.; Perry, S.C.; Mauzeroll, J. Combined spectroelectrochemical and simulated insights into the electrogenerated chemiluminescence coreactant mechanism. *Anal. Chem.* **2018**, *90*, 7377–7382. [CrossRef]

156. Tao, X.L.; Pan, M.C.; Yang, X.; Yuan, R.; Zhuo, Y. CDs assembled metal-organic framework: Exogenous coreactant-free biosensing platform with pore confinement-enhanced electrochemiluminescence. *Chin. Chem. Lett.* **2022**, *33*, 4803–4807. [CrossRef]

157. Xia, S.; Pan, J.; Dai, D.; Dai, Z.; Yang, M.; Yi, C. Design of portable electrochemiluminescence sensing systems for point-of-care-testing applications. *Chin. Chem. Lett.* **2023**, *34*, 107799. [CrossRef]

158. Yin, F.; Yang, E.; Ge, X.; Sun, Q.; Mo, F.; Wu, G.; Shen, Y. Coupling WO_{3-x} dots-encapsulated metal-organic frameworks and template-free branched polymerization for dual signal-amplified electrochemiluminescence biosensing. *Chin. Chem. Lett.* **2024**, *35*, 108753. [CrossRef]

159. Li, C.; Liu, C.; Liu, R.; Wang, Y.; Li, A.; Tian, S.; Cheng, W.; Ding, S.; Li, W.; Zhao, M.; et al. A novel CRISPR/Cas14a-based electrochemical biosensor for ultrasensitive detection of Burkholderia pseudomallei with PtPd@ PCN-224 nanoenzymes for signal amplification. *Biosens. Bioelectron.* **2023**, *225*, 115098. [CrossRef]

160. Gootenberg, J.S.; Abudayyeh, O.O.; Lee, J.W.; Essletzbichler, P.; Dy, A.J.; Joung, J.; Verdine, V.; Donghia, N.; Daringer, N.M.; Freije, C.A.; et al. Nucleic acid detection with CRISPR-Cas13a/C2c2. *Science* **2017**, *356*, 438–442. [CrossRef]

161. Kellner, M.J.; Koob, J.G.; Gootenberg, J.S.; Abudayyeh, O.O.; Zhang, F. SHERLOCK: Nucleic acid detection with CRISPR nucleases. *Nat. Protoc.* **2019**, *14*, 2986–3012. [CrossRef]

162. Peng, S.; Tan, Z.; Chen, S.; Lei, C.; Nie, Z. Integrating CRISPR-Cas12a with a DNA circuit as a generic sensing platform for amplified detection of microRNA. *Chem. Sci.* **2020**, *11*, 7362–7368. [CrossRef] [PubMed]

163. Pan, Y.; Yang, J.; Luan, X.; Liu, X.; Li, X.; Yang, J.; Huang, T.; Sun, L.; Wang, Y.; Lin, Y.; et al. Near-infrared upconversion–activated CRISPR-Cas9 system: A remote-controlled gene editing platform. *Sci. Adv.* **2019**, *5*, eaav7199. [CrossRef] [PubMed]

164. Song, N.; Li, S.; Lv, Z.; Ding, X.; Li, F.; Yang, D. Engineering CRISPR/Cas-based nanosystems for therapeutics, diagnosis and bioimaging. *Chin. Chem. Lett.* **2023**, *34*, 108134. [CrossRef]

165. Chen, Y.; Zhang, Y.; Pan, F.; Liu, J.; Wang, K.; Zhang, C.; Cheng, S.; Lu, L.; Zhang, W.; Zhang, Z.; et al. Breath analysis based on surface-enhanced Raman scattering sensors distinguishes early and advanced gastric cancer patients from healthy persons. *ACS Nano* **2016**, *10*, 8169–8179. [CrossRef] [PubMed]

166. Li, J.; Jiao, Z.; Li, J.; Bai, H.; Xi, G. Plasmonic rhenium trioxide self-assembled microtubes for highly sensitive, stable and reproducible surface-enhanced Raman spectroscopy detection. *Chin. Chem. Lett.* **2023**, *34*, 107572. [CrossRef]

167. Wang, C.; Huang, L.; Wang, S.; Wu, L.; Wang, Y.; Dong, J. A distinction of gliomas at cellular and tissue level by surface-enhanced Raman scattering spectroscopy. *Chin. Chem. Lett.* **2024**, *35*, 109383. [CrossRef]

168. Li, S.; Li, Z.; Hao, Q.; Wang, S.; Yang, Y.; Xu, J.; Yin, Z.; Zhang, L.; Chen, Z. Ultrastable graphene isolated AuAg nanoalloy for SERS biosensing and photothermal therapy of bacterial infection. *Chin. Chem. Lett.* **2024**, *35*, 108636. [CrossRef]

169. Jiang, X.; Jiang, H.; Tang, Y.; Zhang, H.; Yang, L.; Wang, X.; Zhao, B. $g\text{-}C_3N_4/TiO_{2-X}$ heterojunction with high-efficiency carrier separation and multiple charge transfer paths for ultrasensitive SERS sensing. *Chin. Chem. Lett.* **2024**, *35*, 109415. [CrossRef]

170. Tian, S.; Huang, W.; Hu, J.; Wang, H.; Zhang, Z.; Xu, L.; Li, J.; Sun, Y. Exploring the frontiers of plant health: Harnessing NIR fluorescence and surface-enhanced Raman scattering modalities for innovative detection. *Chin. Chem. Lett.* **2024**, *36*, 110336. [CrossRef]

171. Cao, Q.; Li, J.; Wang, E. Recent advances in the synthesis and application of copper Nanomaterials based on various DNA scaffolds. *Biosens. Bioelectron.* **2019**, *132*, 333–342. [CrossRef]

172. Li, R.; Liu, Q.; Jin, Y.; Li, B. Fluorescent enzyme-linked immunoassay strategy based on enzyme-triggered in-situ synthesis of fluorescent copper nanoclusters. *Sens. Actuators B Chem.* **2019**, *281*, 28–33. [CrossRef]

173. Qing, T.; Qing, Z.; Mao, Z.; He, X.; Xu, F.; Wen, L.; He, D.; Shi, H.; Wang, K. dsDNA-templated fluorescent copper nanoparticles: Poly (AT-TA)-dependent formation. *RSC Adv.* **2014**, *4*, 61092–61095. [CrossRef]

174. Fan, K.; Kang, W.; Qu, S.; Li, L.; Qu, B.; Lu, L. A label-free and enzyme-free fluorescent aptasensor for sensitive detection of acetamiprid based on AT-rich dsDNA-templated copper nanoparticles. *Talanta* **2019**, *197*, 645–652. [CrossRef]

175. Wang, Y.; Cui, H.; Cao, Z.; Lau, C.; Lu, J. Additive and enhanced fluorescence effects of hairpin DNA template-based copper nanoparticles and their application for the detection of NAD+. *Talanta* **2016**, *154*, 574–580. [CrossRef] [PubMed]

176. Singh, S.; Singh, M.K.; Das, P. Biosensing of solitary and clustered abasic site DNA damage lesions with copper nanoclusters and carbon dots. *Sens. Actuators B Chem.* **2018**, *255*, 763–774. [CrossRef]

177. Carrillo-Torres, R.; García-Soto, M.; Morales-Chávez, S.; Garibay-Escobar, A.; Hernández-Paredes, J.; Guzmán, R.; Barboza-Flores, M.; Álvarez-Ramos, M. Hollow Au–Ag bimetallic nanoparticles with high photothermal stability. *RSC Adv.* **2016**, *6*, 41304–41312. [CrossRef]

178. Wang, J.; Wang, W.; Yang, L.; Zhao, J.; Han, G.; Yu, X.; ShenTu, X.; Ye, Z. Surface engineered bimetallic gold/silver nanoclusters for in situ imaging of mercury ions in living organisms. *Anal. Bioanal. Chem.* **2022**, *414*, 4235–4244. [CrossRef] [PubMed]

179. Liu, L.; Mu, X.; Liu, H.; Wang, Q.; Bai, X.; Wang, J.; Liu, H.; Xu, F.; Jing, Y.; Dai, H.; et al. Structure, Luminescence, and bioimaging of bimetallic CuAu nanoclusters. *Opt. Mater.* **2018**, *86*, 291–297. [CrossRef]

180. Tothill, I.E. Biosensors for cancer markers diagnosis. *Semin. Cell Dev. Biol.* **2009**, *20*, 55–62. [CrossRef] [PubMed]